RSC Advances

REVIEW

View Article Online
View Journal | View Issue

Cite this: *RSC Adv.*, 2025, **15**, 26710

Recent advances in metal–organic frameworks for antibacterial applications: mechanisms and emerging strategies

Yuan Tian,[ab] Bin Wang,[ab] Zerun Zhang,[ab] Tianhan Kai,[ab] Pian Wu*[ab] and Ping Ding*[ab]

Received 27th April 2025
Accepted 9th July 2025

DOI: 10.1039/d5ra02955d

rsc.li/rsc-advances

Bacterial infections represent a significant and ongoing challenge to public health worldwide. Metal–organic frameworks (MOFs), owing to their distinctive structural features and tunable physicochemical properties, have demonstrated considerable potential in antibacterial applications. Extensive research has been conducted to explore the application of MOFs in antimicrobial contexts. This review systematically examines the underlying antibacterial mechanisms of MOFs, including the release of metal ions, the generation of reactive oxygen species (ROS), and physical disruption of microbial membranes. Furthermore, it also discussed the specific applications of MOFs against various bacterial species and evaluates their prospective roles in the development of advanced antibacterial strategies.

1. Introduction

Bacterial infections have become the second leading cause of mortality globally. In 2019, it was reported that 33 pathogens caused 7.7 million of 13.7 million infection-related deaths.[1] The widespread misuse and overuse of antibiotics have contributed to the rapid emergence of antibiotic resistance, presenting a critical threat to global public health.[2–4] In response to this challenge, a range of novel antibacterial strategies has been developed, including physical and chemical approaches such as photodynamic and photothermal therapies,[5–7] immunoengineering techniques involving antibacterial peptides and bacteriophages,[8] and nanotechnology-based methods employing metal nanoparticles.[9] Among these, nanomaterials have garnered significant attention due to their enhanced antibacterial properties. However, traditional antibacterial nanomaterials, such as silver nanoparticles, are often suffer from limitations including aggregation and reduced activity. Similarly, single-component photocatalytic materials like TiO_2 and ZnO are heavily dependent on external light sources, limiting their efficacy in dark or complex environments.[10] In contrast, the advent of MOFs has shown promise in overcoming these drawbacks, offering more versatile and effective antibacterial solutions.[11]

MOFs are porous crystalline materials characterized by their exceptionally high porosity and large internal surface area, formed through the coordination of metal ions or clusters with organic ligands.[12–15] The structural tunability of MOFs-achieved by modifying the metal centers, ligand types, and synthesis conditions-enables the development of frameworks with tailored functionalities. Due to these properties, MOFs have found increasingly application in diverse antibacterial contexts, including as antimicrobial coatings for medical devices to inhibit biofilm formation by drug-resistant bacteria, as active components in food packaging to prevent microbial contamination and prolong shelf life, and as ingredients in oral care products to combat dental pathogens and plaque. It is of great significance to strengthen the summary of MOFs in the antibacterial field.

While existing reviews on MOFs have largely concentrated on their structural features and functional modifications, comprehensive analyses of their antibacterial mechanisms remain limited.[16–18] To address this gap, the present review focuses primarily on elucidating the antibacterial mechanism of MOFs, specifically through key pathways such as metal ions release, ROS generation, and physical interactions that disrupt bacterial integrity (Scheme 1). In addition, the review explores the application of MOFs against various bacterial strains, including Gram-negative, Gram-positive, and multidrug-resistant bacteria. Finally, the current challenges and prospects of MOFs in antibacterial applications were discussed. This systematic and comprehensive review aims to provide an important foundation for subsequent research on the antibacterial applications of MOFs.

2. Antibacterial mechanism of MOFs

2.1 Release of metal ions

The use of metal ions for antibacterial purposes is a well-established and extensively studied strategy. Metal ions, such

[a]Xiangya School of Public Health, Central South University, Changsha, Hunan, 410078, China. E-mail: wupian@csu.edu.cn; pingshui@csu.edu.cn
[b]Hunan Provincial Key Laboratory of Clinical Epidemiology, Changsha, Hunan, 410078, PR China

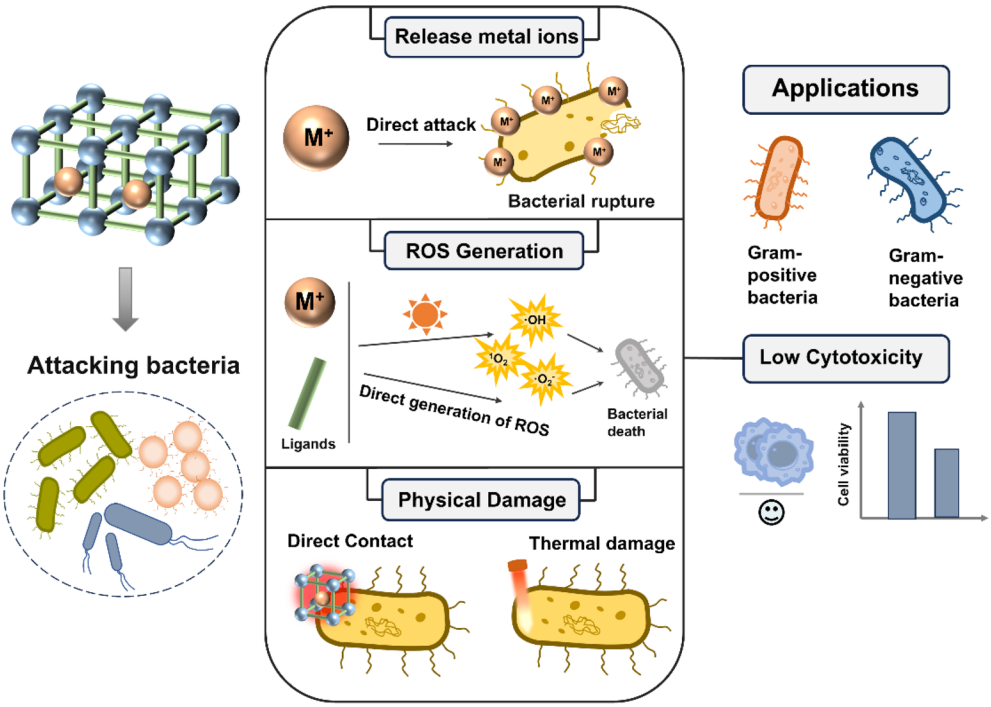

Scheme 1 Schematic diagram of MOFs antibacterial mechanisms and applications.

as Ag^+, Cu^{2+}, Zn^{2+}, Co^{2+} and Fe^{2+}/Fe^{3+} exhibit potent bactericidal activity. These positively charged metal ions interact electrostatically with the negatively charged bacteria cell walls, disrupting membrane integrity by interacting with membrane proteins and the phospholipid bilayer. Furthermore, they can penetrate bacterial cells, bind to DNA, thereby hindering replication and transcription, inactivate essential enzymes, and generate ROS through redox processes, all of which contribute to bacterial cell death.[19,20] At present, significant research has been devoted to incorporating metal ions into MOFs. MOFs serve as carriers that regulate ion release, maintaining antibacterial effects while minimizing toxicity (Fig. 1).

Ag^+ is particularly notable for its broad-spectrum activity. Ag^+ primarily binds to sulfhydryl (–SH) groups on membrane proteins, disrupting protein structure and function, increasing membrane permeability, and causing intracellular leakage. Additionally, Ag^+ can enter bacterial cells, where it interferes with nucleic acid function and inhibits respiratory chain enzymes, ultimately leading to cell death.[21–24] However, the unregulated release of Ag^+ can damage normal tissues. Numerous studies have explored the combination of Ag^+ with MOFs to control the release of Ag^+. Ning *et al.* synthesized two Ag-based MOFs [Ag_2 (O-IPA) (H_2O)–(H_3O)] (compound 1) and [Ag_5 (PYDC)$_2$ (OH)] (compound 2) by coordinating Ag^+ with aromatic carboxylic acids containing hydroxyl and pyridine groups.[25] These structures enabled controlled Ag^+ release. Mechanism studies revealed that upon approaching bacterial surfaces, the MOFs released Ag^+, disrupting ion balance and membrane integrity. The Ag^+ also penetrated bacterial cells and interacted with peptidoglycan and phospholipid components, causing further cellular damage. Binding of Ag^+ to protein sulfhydryl groups led to enzyme inactivation and eventual bacterial death. The minimum inhibitory concentrations (MICs) for compounds 1 and 2 against *Escherichia coli* (*E. coli*) were 5–10 ppm and 10–15 ppm, respectively, while those against *Staphylococcus aureus* (*S. aureus*) were 10–15 ppm and 15–20 ppm, respectively. To further reduce Ag^+-associated cytotoxicity, Guo *et al.* encapsulated Ag nanoparticles within a spherical Cu-TCPP MOF. Toxicity assessments using the MTT assay demonstrated that the half-maximal inhibitory concentration (IC50) values of Ag-CuTCPP MOFs, Ag nanoparticles and Ag^+ aqueous solution were 50.33 μg mL^{-1}, 6.55 μg mL^{-1} and 2.12 μg mL^{-1}, respectively, indicating significantly reduced cytotoxicity in the MOF-based system.[26] The antibacterial mechanism was attributed to Ag^+ release, which compromised bacterial membrane integrity and caused intracellular content leakage.

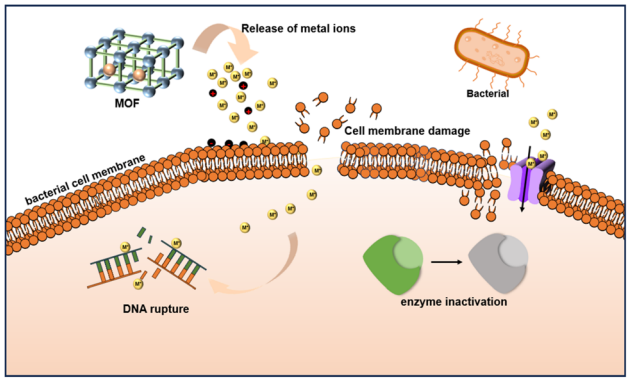

Fig. 1 Schematic illustration of the antibacterial mechanism of MOFs *via* the controlled release of metal ions targeting bacterial cells.

The MICs for Ag-CuTCPP MOF against *E. coli*, *Bacillus subtilis* (*B. subtilis*), and *S. aureus* were 12.50 μg mL^{-1}, 6.25 μg mL^{-1}, and 6.25 μg mL^{-1}, respectively. These findings underscore the potential of MOF-based platforms to effectively control metal ion release, maintain high antibacterial efficiency, and minimize cytotoxicity.

In addition to the Ag^{+}, copper ions (Cu^{2+}) exhibit diverse and potent antibacterial activities. Cu^{2+} possesses intrinsic antimicrobial properties and exerts its effects by penetrating bacterial cells, disrupting intracellular functions, and interfering with metabolic processes. Furthermore, Cu^{2+} can catalyze the generation of hydroxyl radicals (·OH), which contribute to membrane rupture and cellular damage.[27,28] Previous studies have demonstrated that copper-coated surfaces in clinical environments can effectively reduce microbial contamination. Copper can function as a standalone antibacterial agent or be integrated into composite materials through coordination with various ligands to enhance its efficacy.[29–31] Compared to Ag-MOFs, Cu-MOFs typically demonstrate lower antibacterial potency, but pose a reduced risk of bioaccumulation relative to Ag^{+}. To address the limitations of Ag^{+} toxicity and enhance the antibacterial performance of Cu-MOFs, Guo *et al.* developed a polyer-modified MOF composite, Cu-MOF@AgNPs.[32] This material incorporates polymeric MOFs (polyMOFs), which offer improved structural stability. Antibacterial assays revealed that Cu-MOF@AgNPs significantly reduced bacterial viability within 6 h. However, bacterial regrowth occurred thereafter, indicating incomplete eradication. In contrast, polyCu-MOF@AgNPs achieved complete inhibition of *S. aureus* and *E. coli* within 10 h, with a MIC of approximately 10 μg mL^{-1}. Biocompatibility assessments indicated no significant cytotoxicity within the concentration range of 2–20 μg mL^{-1}. These findings underscore the importance of structural modification and composite strategies in enhancing MOF-based antibacterial performance. To better control the release of Cu^{2+}, Zheng *et al.* coated Cu-MOF-74 onto a polyvinylidene fluoride (PVDF) membrane.[33] The modified membrane achieved a maximum Cu^{2+} release concentration of 0.42 mg L^{-1} (when coated with 0.025 g Cu-MOF-74), sustaining release for up to one week. This system also facilitated ·OH generation, contributing to enhanced bactericidal activity. The membrane demonstrated robust antibacterial performance against *E. coli*, achieving an inhibition rate of 97.7%. Additionally, Cu-MOF can be chemically modified to augment their antibacterial properties. Studies have shown that Cu^{2+} ions can coordinate with functional groups such as amino, carboxyl, or sulfhydryl groups. In this context, Xiao *et al.* designed an L-cysteine-modified Cu-MOF nanofiber (L-cys@Cu MOF), leveraging Cu–S and Cu–N coordination bonds.[34] The nanofiber effectively disrupted bacterial membranes, allowing Cu^{2+} to penetrate and interact with intracellular DNA, ultimately leading to bacterial cell death. Cytotoxicity evaluation confirmed that the nanofiber fabric was biocompatible and safe for application on human skin.

Zinc is also a metal ion recognized for its potent antimicrobial properties. Yuan *et al.* synthesized a Zn-MOF that demonstrated notable antibacterial efficacy, with inhibition zone diameters of 12.22 mm against *E. coli* and 10.10 mm against *S. aureus*.[35] Despite its antimicrobial effectiveness, the biocompatibility of Zn-MOFs remains a critical consideration in their biomedical application. Chen *et al.* addressed this issue by developing a Zn-BTC, which effectively inhibited the growth of Methicillin-resistant *S. aureus* (MRSA) and *E. coli* through the controlled release of Zn^{2+}. Biocompatibility was evaluated using the CCK-8 assay, revealing a marked decrease in cell viability at a Zn $(NO_3)_2$ concentration of 5 μg mL^{-1}, with significant cytotoxicity observed at 50 μg mL^{-1}. In contrast, Zn-BTC at the same concentration induced minimal cell death, suggesting that the MOF structure successfully moderated Zn^{2+} release and mitigated cytotoxic effects. These findings underscore the necessity of avoiding high concentrations of unbound Zn^{2+}, which can be detrimental to healthy cells. To further enhance both biocompatibility and therapeutic efficacy, Yao *et al.* developed a microneedle (MN) array incorporating Zn-MOF within a hyaluronic acid methacrylate (MeHA).[36] This system facilitated sustained Zn^{2+} release and ROS generation, contributing to efficient bacterial inactivation. Cytotoxicity assays, including CCK-8 and live/dead staining, indicated that when ZIF-8 nanoparticle concentrations were maintained below 3 mg mL^{-1}, the system exhibited minimal cytotoxicity. This approach exemplifies the potential of integrating Zn-MOFs with biocompatible carriers to improve biosafety and therapeutic outcomes.

Beyond Ag^{+}, Cu^{2+}, and Zn^{2+}, MOFs incorporating other metal centers such as Fe, Zr, Ti, Al, and Ce have also been explored for antibacterial applications. A comparative study assessing the antibacterial activities of Cu-MOF, Fe-MOF, and Zr-MOF found that Cu-MOF achieved complete inactivation of *E. coli* under both dark and illuminated conditions. In contrast, Fe-MOF exhibited only 2.47% antibacterial activity in darkness, which increased modestly to 4.94% upon exposure to light. Zr-MOF showed no activity in the dark but reached 73.56% efficacy under illumination.[37] These findings highlight the light-responsive behavior of certain MOFs, particularly those containing Zr and Ti, which often rely on photocatalytically generated ROS to exert antibacterial effects.[38,39] Iron-based MOFs (Fe-MOFs) are frequently employed in synergistic systems to enhance antibacterial efficacy. For example, Prachi *et al.* incorporated gentamicin into an Fe-BDC MOF, where the antibacterial activity was attributed to a non-photocatalytic Fenton-like reaction involving Fe^{3+} ions and ·OH generation.[40] The gentamicin-loaded Fe-MOF exhibited an inhibition zone of 34 ± 1.7 mm against *S. aureus* at a concentration of 1 mg mL^{-1}, double that of gentamicin alone. Zr-MOFs, on the other hand, demonstrated significant photo-induced antibacterial properties, further supporting the potential of ROS-mediated mechanisms in such systems. The detailed pathways and design considerations of these ROS-generating MOFs will be elaborated in subsequent sections of this article.

Overall, MOFs exhibit robust antibacterial performance primarily through the release of metal ions that disrupt bacterial membranes and interfere with intracellular functions. MOFs incorporating Ag^{+}, Cu^{2+}, Co^{2+}, and Zn^{2+} are particularly effective. However, their strong antibacterial activity often comes with the risk of cytotoxicity due to uncontrolled or prolonged metal ion release. To address this, recent research has

focused on surface modifications, structural engineering, and composite designs aimed at regulating ion release, thus improving therapeutic safety and efficiency. While the bactericidal mechanism *via* metal ion release is well-documented, the interfacial interactions between MOFs and bacterial membranes-especially electrostatic interactions-remain relatively underexplored. Given that bacterial membranes are typically negatively charged, positively charged MOFs or their metal centers are expected to rapidly bind through electrostatic attraction, potentially influencing both adhesion and antimicrobial activity. Yet, this aspect has received insufficient attention in the current literature. Future studies investigating the influence of surface charge, such as by tuning the zeta potential of MOFs or accounting for variations in bacterial membrane composition, may reveal new strategies for optimizing MOF-based antibacterial systems.

2.2 Reactive oxygen species generation

ROS are highly reactive oxygen-containing molecules, including hydrogen peroxide (H_2O_2), superoxide ($\cdot O_2^-$), ·OH, and singlet oxygen ($^1O_2$), Their antibacterial activity primarily arises from their capacity to damage essential cellular components, such as DNA, proteins, and lipids.[41,42] ROS can also compromise bacterial viability by attacking the peptidoglycan layer of the cell wall, thereby inducing structural instability and ultimately leading to cell death.[43,44] MOFs, composed of metal ions/clusters coordinated with organic ligands, possess unique structural features that enable the controlled generation of ROS through various mechanisms. These mechanisms can be broadly classified into three categories: (1) metal-centered ROS generation, where the redox activity of metal nodes catalyzes ROS formation; (2) ligand-mediated ROS generation, where photo or chemically active ligands contribute to ROS production; and (3) metal–ligand synergistic mechanisms, which leverage cooperative interactions between metal centers and organic linkers to enhance ROS output. In the following sections, we will examine each of these ROS-generating mechanisms in detail, highlighting their distinct reaction pathways, optimal activation conditions, and relevant biomedical or environmental application scenarios.

2.2.1 Based on metal centers. Metal centers within MOFs, such as Cu, Fe, Ce, can generate ROS through catalytic processes, These ROS, including ·OH, $\cdot O_2^-$, and $^1O_2$, possess strong oxidative potential and can effectively disrupt bacterial cell membranes, denature proteins, and damage nucleic acids, thereby exerting potent antibacterial effects (Fig. 2).

Under varying environmental conditions, MOFs exhibit diverse ROS generation mechanisms and corresponding antibacterial behaviors. In recent years, researchers have developed a range of representative MOFs capable of finely regulating ROS production through strategic modifications of their metal centers, organic ligands, and pore architectures, thereby significantly enhancing their antimicrobial efficacy. For example, Huang *et al.* reported a hierarchically porous cerium metal–organic framework (Ce-MOF), in which cerium ions in Ce-MOFs serve as Lewis acid sites to catalyze the conversion of

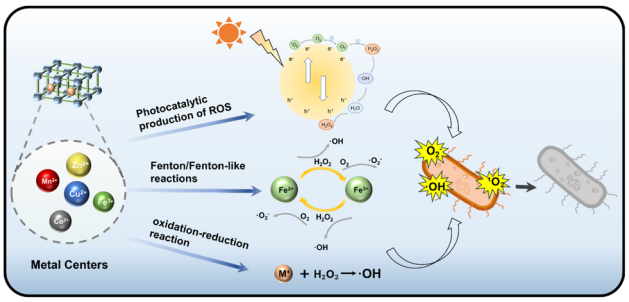

Fig. 2 Schematic diagram of the antibacterial mechanism of MOFs generating ROS based on metal centers.

atmospheric oxygen into highly reactive ROS. Notably, the catalytic activity of this Ce-MOF was approximately 1800 times greater than that of conventional CeO_2.[45] The demonstrated the ability to autonomously catalyze the generation of $\cdot O_2^-$ and ·OH from molecular oxygen, achieving nearly complete bacterial inactivation under ambient temperature and pressure, without the need for light, chemical additives, or specific humidity conditions. In addition, the dendritic surface morphology and hierarchical pore-channel structure of Ce-MOFs facilitated improved accessibility to catalytical sites and enhanced electrostatic interactions with bacterial cells, particularly those with positively charged surfaces. This structural design enabled close contact between bacteria and short-lived ROS, thus maximizing bactericidal efficiency.

In addition to Ce-MOFs, Cu-MOFs have also attracted significant interest due to their inherent stability and notable antibacterial performance. Cu^{2+} within Cu-MOFs can trigger a cascade of redox reactions in the presence of substances, such as H_2O_2. Specifically, Cu^{2+} acts as a catalytic center facilitating the decomposition of H_2O_2 *via* a Fenton-like mechanism. During this process, Cu^{2+} is reduced to Cu^+ through electron transfer, while H_2O_2 is oxidized to produce highly reactive ·OH. The resultant Cu^+ can further react with additional H_2O_2, sustaining a continuous cycle of ROS production. These ROS, particularly ·OH, are potent oxidizing agents that disrupt the structural integrity of cell membranes, leading to pore formation, leakage of intracellular ions such as K^+, Ca^{2+}, osmotic imbalance and ultimately cell swelling and lysis.[27,46] For example, Wang *et al.* designed a 2D Cu-MOF NSs exhibiting intrinsic peroxidase (POD)-like activity, capable of catalyzing H_2O_2 to generate ·OH. This material not only facilitates ROS production but also offers abundant Cu^{2+}/Cu^+, redox-active surface sites, contributing to its potent antibacterial performance. However, in practical applications, the presence of environmental anions such as phosphate (PO_4^{3-}) and carbonate (CO_3^{2-}) can lead to precipitation with Cu^{2+} ions, thereby reducing their effective concentration and diminishing the material's antibacterial efficacy.[47]

The Fenton reaction represents a fundamental chemical process for the generation of ROS. This action involves the catalytic decomposition of H_2O_2 by transition metal ions, such as Fe^{2+}, Cu^+, resulting in the formation of highly reactive ·OH. Within the context of MOFs, iron-based MOFs, such as MIL-101

(Fe), can efficiently generate ·OH through the Fenton reaction. The underlying mechanisms include redox reactions: Fe^{2+} + H_2O_2 → Fe^{3+} + ·OH + OH^-, and Fe^{3+} + $\cdot O_2^-$ → Fe^{2+} + O_2. In a study conducted by Peng *et al.*, MIL-101(Fe) was synthesized and subjected to thermal treatment under an inert helium atmosphere to modulate the Fe^{2+}/Fe^{3+} ratio at the coordinatively unsaturated iron sites (Fig. 3A).[48] This treatment enhanced the material's electron transfer capabilities and increased the density of active sites. The resulting material was capable of adsorbing molecular oxygen on its surface, thereby facilitating ROS generation for the disruption of bacterial cell membranes and inducing cell death. Beyond leveraging the intrinsic Fenton or Fenton-like catalytic properties of MIL-101(Fe) for antibacterial applications, subsequent studies have augmented its therapeutic potential by integrating the antimicrobial peptide LL-37 and the antibiotic Vancomycin to construct a multifunctional antibacterial nanoplatform (Fig. 3B).[49] This composite system maintains the capacity of MIL-101(Fe) to catalyze endogenous H_2O_2 into cytotoxic ·OH under the mildly acidic and oxidative microenvironment characteristic of bacterial infections, thereby inducing oxidative stress in bacterial cells. Concurrently, LL-37 facilitates membrane disruption, while Vancomycin inhibits cell wall biosynthesis, establishing a synergistic, multi-mechanistic antibacterial approach. Additionally, the incorporation of LL-37 imparts bacterial targeting and near-infrared (NIR) imaging capabilities. Compared to the use of MIL-101(Fe) alone, this integrated strategy exhibits superior antibacterial efficacy, particularly against multidrug-resistant strains such as MRSA, and offers potential for real-time monitoring during therapeutic intervention.

Light conditions can significantly enhance the ROS generating capabilities of MOFs.[52] Under photocatalytic conditions, metal nodes within MOFs absorb photons, facilitating the excitation of electrons from the valence band to the conduction band, thereby generating electron–hole pairs. The resulting holes can oxidize surrounding substrates to generate ROS such as O_2^- or ·OH.[53] Zhao *et al.* reported a method for assembling UiO-66 particles onto the substrate surface *via* a visible-light-assisted process in the presence of dopamine (DA) (Fig. 3C).[50] In this system, visible light irradiation induces ROS production from UiO-66, which in turn catalyzes the oxidative polymerization of dopamine, leading to the formation of a dense, uniform, and stable MOF membrane. This membrane exhibited rapid photodynamically induced bactericidal activity against Gram-positive *S. aureus* and Gram-negative *E. coli* under visible light. The enhancement of photocatalytic activity under light conditions is attributed to separation and transfer of photo-generated charge carriers, thereby significantly increasing ROS generation and antibacterial efficacy. Furthermore, cellular experiments and hemocompatibility assessments using fresh rat blood confirmed the favorable biocompatibility of the system, indicating its potential for biomedical applications.

In addition to monometallic systems, the incorporation of bimetallic centers within MOFs offers additional advantages for ROS generation through a synergistic catalytic mechanism, thus enhancing both efficiency and selectivity. For example, Wen *et al.* reported a novel Co–Fe bimetallic MOF with coordinatively unsaturated active sites.[54] Due to cobalt's higher electronegativity relative to iron, electron transfer from the aromatic ligand to the metal centers is facilitated, resulting in polarization of the electron distribution and improved H_2O_2 activation. This mechanism leads to the efficient generation of ·OH, which disrupts bacterial cell membranes, proteins, and culminating in potent antibacterial activity.

To further advance MOFs functionality, researchers have encapsulated quantum dots (QDs) into ZIF-8 frameworks to construct QDs@ZIF-8 composite materials (Fig. 3D).[51] Under visible light irradiation, ZAIS QDs are photoexcited to generate electron–hole pairs. A Zn–S bond formed at the QD-ZIF-8 interface facilitates electron transfer from the QDs to the ZIF-8 matrix, thereby enhancing ROS generation. The high specific surface area and porosity of ZIF-8 not only allow for

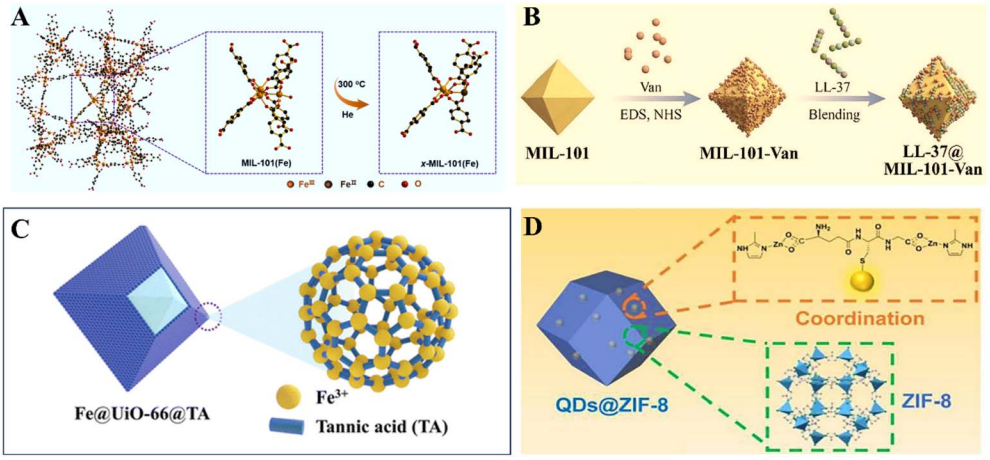

Fig. 3 Schematic diagrams of some MOFs structures (A) evolution of coordinatively unsaturated Fe sites in MIL-101 (Fe) after thermal treatment at 300 °C in He atmosphere (reprinted with permission from ref. 48 Copyright 2022 Elsevier). (B) LL-37@MIL-101-Van (reprinted with permission from ref. 49 Copyright 2022 Elsevier). (C) Fe@UiO-66@TA (reprinted with permission from ref. 50 Copyright 2024 Royal Society of Chemistry). (D) QDs@ZIF-8 (Reprinted with permission from ref. 51 Copyright 2021 Elsevier).

greater O_2 adsorption but also inhibit QD aggregation, thereby maintaining photocatalytic efficiency. This system exhibited remarkable antibacterial performance, achieving 99.99% inactivation of *E. coli* within 60 min and 99.99% inactivation of *S. aureus* within 120 min.

ROS generation mechanism mediated by metal centers constitutes a foundational mechanism underlying the antibacterial activity of MOFs. The intrinsic catalytic properties of these metal sites, when augmented by light irradiation, markedly enhance ROS production and thus significantly improve the antibacterial performance of MOFs.

2.2.2 Based on ligands. In MOFs, organic ligands serve not only as structural linkers that coordinate with metal centers to form a stable framework structure, but also play active roles in the antibacterial process through a variety of mechanisms (Fig. 4). Notably, certain ligands contribute directly to the generation of ROS, thereby enhancing the antibacterial efficacy of the material. The chemical composition, structural characteristics, and degree of functionalization of the ligands significantly influence the overall antibacterial performance of MOFs.

Photoresponsive ligands function as photosensitizers, facilitating the conversion of light energy into cytotoxic ROS *via* electron transfer mechanisms. The extensive π-conjugation present in porphyrins enables strong absorption the visible-light and results in high $^1O_2$ quantum yields.[55–57] For example, Zhou *et al.* synthesized azidized Zn(II)-based porphyrin by integrating porphyrin moieties into a surface anchored MOF (SURMOF) structure, further developing SURGEL thin films.[58] This SURGEL film demonstrated potent antibacterial activity under visible light irradiation by generating $^1O_2$, significantly reducing the survival rate of *E. coli* to 2.29%. To overcome limitations in antibacterial efficiency associated with single-ligand systems, Xu *et al.* utilized a dual-ligand strategy incorporating porphyrins and ammonium glycyrrhizinate (AG) within Zr-MOFs.[38] This design combined the membrane-disrupting capabilities of porphyrins with the bacterial membrane synthesis-inhibiting capability of AG, resulting in enhanced ROS generation under photodynamic conditions synergistic antibacterial effects. The resulting materials demonstrated superior antibacterial performance against *E. coli*, *S. aureus*, and *B. subtilis*, achieving sterilization efficiencies exceeding 99.99% under simulated light conditions and maintaining over 98.12% efficacy after 60 days of storage. Porphyrin-based photoresponsive ligands remain among the most extensively studied for antimicrobial applications due to their high ROS generation efficiency, light-triggered activation, and controllable responsiveness. However, their reliance on external light sources imposes constraints on their clinical applicability, particularly in treating deep-seated infections. The limited tissue penetration of light restricts their bactericidal efficacy in internal or occluded environments.

In contrast, non-photoactive ligands bearing redox moieties can induce oxidative stress *via* metal–ligand electron transfer, enabling antimicrobial activity without the need for light activation. Phenolic ligands such as gallic acid (GA) exhibit inherent antioxidant and can generate ROS under certain conditions. Sandy *et al.* prepared a Cu-GA MOF by incorporating GA, capitalizing on GA's capacity to disrupt bacterial membranes and promote ROS-mediated oxidative stress.[59] This material demonstrated effective inhibition of *E. coli* and *Lactobacillus*. Beyond porphyrin, other ligand classes, such as phenolic ligands, carboxylic acid (*e.g.*, terephthalic acid), azole derivatives (*e.g.*, 2-methylimidazole), and thiols (mercaptobenzoic acid), can also promote ROS generation through

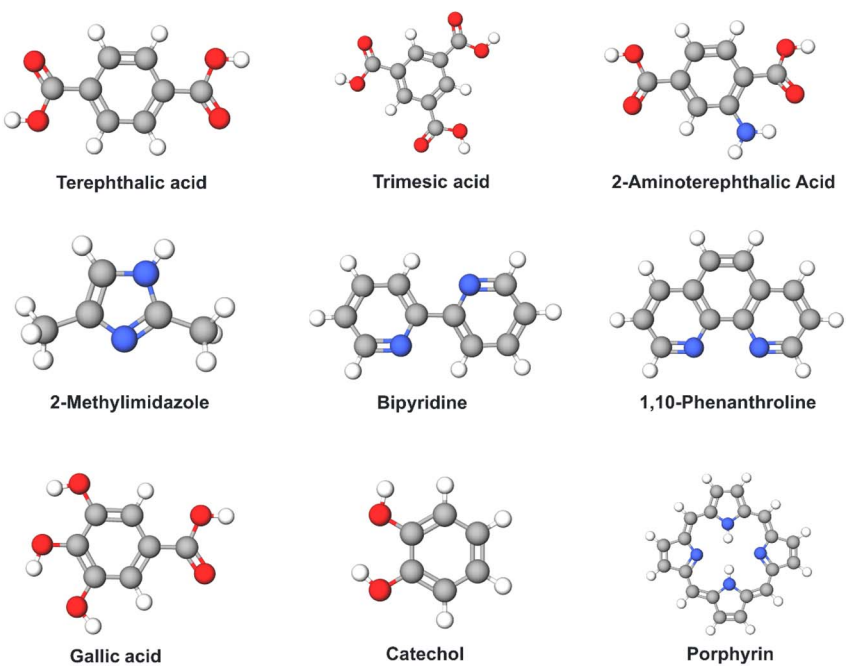

Fig. 4 Some common MOFs ligands capable of producing or promoting the production of ROS.

spontaneous or metal–ligand-mediated electron transfer mechanisms. These non-photoresponsive systems are particularly advantageous for applications in dark or *in vivo* environments, although their antimicrobial efficacy is typically lower than that of photoactivated systems.

Ligand functionalization presents an additional strategy to enhance MOF-based antibacterial activity. The incorporation of specific functional groups, such as quaternary ammonium salts and imidazole, can significantly augment antibacterial performance. Quaternary ammonium group, for example, confer positive surface charge, enabling electrostatic interactions with negatively charged bacterial membranes, which in turn enhances membrane disruption and facilitates localized ROS generation. Moreover, quaternary ammonium-functionalized MOFs can efficiently produce ·OH under light exposure, leading to oxidative damage of bacterial membranes, proteins, and nucleic acids. Zhou *et al.* reported a quaternary ammonium-functionalized Fe-TCPP MOF exhibiting over 90% antibacterial efficiency against *P. aeruginosa* under 650 nm laser irradiation, with MIC and minimum bactericidal concentration (MBC) of 512 mg mL^{-1} and 1024 mg mL^{-1}, respectively.[60] These multifunctional ligands contribute to the growing interest in composite antimicrobial mechanisms, including surface-contact killing, ROS co-generation, and metal ion release. However, the synthetic complexity of such multifunctional systems may compromise material stability and scalability.

Furthermore, the electronic characteristics of ligands can modulate the catalytic activity of the metal centers, thus influencing ROS generation efficiency. For example, adjusting the electron-withdrawing properties of pyrazole bridging units has been shown to enhance the photoelectrochemical behavior and ROS yield of MOFs.[61]

Overall, organic ligands contribute to MOF-based antimicrobial activity primarily through photodynamic and redox pathways. The strategic selection and functionalization of ligands are critical in optimizing MOF performance for antibacterial applications. Nevertheless, research into ligand-specific antibacterial mechanisms remains limited. Future studies should aim to deepen our understanding of ligand functionalities, offering new avenues to enhance the efficacy and versatility of MOF-based antimicrobial systems.

2.2.3 The combined action of the metal center and the ligand. The interaction between metal centers and organic ligands in MOFs not only facilitates efficient ROS generation but also enhances antibacterial efficacy through multiple mechanisms.[62] One such mechanism involves ligand–metal charge transfer (LMCT), which enables ROS production in the absence of external stimuli. For example, Wang *et al.* reported a Zn@MOF system designed for antibacterial application (Fig. 5A).[63] In this core–shell structure based on Zn@MOF, the zinc nucleus functions as an electron reservoir capable of injecting electrons into the surrounding MOF, thereby creating catalytically active zinc sites. The intrinsic porosity of MOF allows the diffusion of water and oxygen molecules to the core–shell interface, where they undergo reduction at the zinc active sites to form ROS. Specifically, the MOF shell modulates the formation of $\cdot O_2^-$ and ·OH through O_2/H_2O reduction pathways, resulting in effective antibacterial action. The biocompatibility of the Zn@MOF was also systematically evaluated. Cytotoxicity assays indicated no significant reduction in cell viability upon treatment. Furthermore, *in vivo* hemolysis experiments using murine red blood cells demonstrated that Zn@MOF did not induce hemolysis even at concentrations up to 2000 μg mL^{-1}. These findings collectively highlight the favorable biocompatibility of Zn@MOF, making it a promising candidate for biomedical antibacterial applications.

Electron transfer is one of the key steps in the generation of ROS, particularly under light irradiation.[68] This process is often facilitated by the interaction between metal centers and ligands, which promotes charge transfer under photonic excitation. For instance, Wang *et al.* developed a the MoS_2/MnS composite in which light-induced significantly enhanced ROS generation (Fig. 5B).[64] Upon visible light exposure, the system exhibited potent antibacterial activity, effectively inactivating over 99% of *E. coli* and *S. aureus* within 120 min. Similarly, Yang *et al.* combined Prussian blue (PB) with MoS_2 to form a core–shell structure (MoS_2@PB), wherein an interfacial electric field is formed between PB and MoS_2.[65] This electric field promotes the separation and migration of photogenerated charge carriers, thereby improving the photocatalytic performance and enhancing ROS production (Fig. 5C). Additionally, MoS_2@PB exhibits strong photothermal effects under 660 nm irradiation, resulting in rapid localized high temperature increases. The generated heat disrupts bacterial membranes and increases permeability, further enhancing antibacterial efficiency. Antibacterial assays demonstrated that after 20 min of light exposure, the antibacterial rates against *S. aureus* for PB, MoS_2, and MoS_2@PB were 64.97%, 53.63%, and 99.73%, respectively, corresponding rates against *E. coli* were 76.84%, 71.93%, and 99.58%. These results underscore the superior antibacterial performance of the MoS_2@PB composite. Importantly, cytocompatibility assessments confirmed that MoS_2@PB maintained cell viability above 90%, indicating excellent biocompatibility.

The formation of stable coordination bonds between ligands and metal center also plays a pivotal role in enhancing the photocatalytic activity of MOFs and promoting ROS generation. For example, Fig. 5D shows a ZIF-8 encapsulating a photosensitizer (SQ), which produces $^1O_2$ under red-light (650 nm) excitation.[66] The microporous architecture of ZIF-8 prevents aggregation of SQ, thereby sustaining its photo reactivity and enabling controlled release to maximize ROS yield. Dimethylimidazole, a commonly used ligand in such systems, exhibits strong coordination with various metal centers. Huang *et al.* utilized 2-methylimidazole and Co^{2+} to synthesize a robust three-dimensional framework (ZIF-67), which effectively modulates the electronic structure of Co^{2+} to catalyze the ·OH generation from H_2O_2 (Fig. 5E).[67]

The interaction between ligands and metal centers within MOFs significantly contributes to their antibacterial performance. In certain systems, ligand-to-metal charge transfer mechanisms regulate the redox potential of the metal centers, facilitating reactions with molecular oxygen and water to generate ROS, such as ·OH. Additionally, ligands can enhance

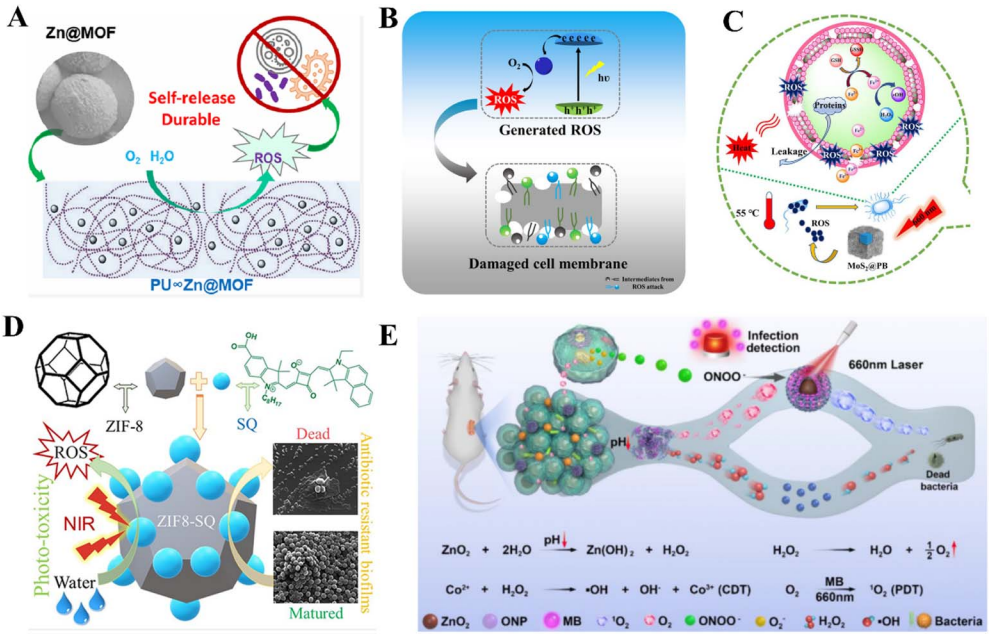

Fig. 5 Metal centers of MOFs with ligands combined with antibacterial. (A) Antibacterial schematic of ROS release from Zn@MOF (reprinted with permission from ref. 63 Copyright 2023 American Chemical Society). (B) Electron transfer occurs between the metal center and the ligand (reprinted with permission from ref. 64 Copyright 2022 Elsevier). (C) The formation of the interfacial electric field between PB and MoS_2 generates ROS to attack bacteria (reprinted with permission from ref. 65 Copyright 2023, Elsevier). (D) ZIF-8 encapsulated with photosensitizer generates ROS to attack bacteria. (Reprinted with permission from ref. 66 Copyright 2019 American Chemical Society). (E) Adjustment of the electronic structure of Co^{2+} to promote its ROS production (reprinted with permission from ref. 67 Copyright 2022, Elsevier).

the light-harvesting capacity and the $^1O_2$ production efficiency of MOFs under irradiation by modulating the photonic absorption and electron excitation properties of the metal centers. Furthermore, ligand-induced modifications MOF structure-such as changes in porosity, stability, and metal ion release kinetics-can influence bacterial interaction modes and overall antimicrobial activity. These synergistic effects between ligands and metal centers are therefore crucial for optimizing the design and functionality of MOF-based antibacterial systems.

2.3 Physical stimulus

In addition to the chemical antibacterial mechanisms discussed previously, physical antibacterial strategies exert their effects by disrupting bacterial structures or interfering with cellular metabolism through the intrinsic physical properties of materials. These approaches present notable advantages, including the mitigation of antibiotic resistance and enhanced environmental compatibility. Physical antibacterial mechanisms generally function *via* two pathways (Fig. 6): (1) direct physical disruption of bacterial membranes upon contact with the material surface, and (2) thermal damage induced by external energy stimuli.

2.3.1 Direct interaction with bacteria. Certain MOFs exhibit inherent physical antibacterial properties by mechanically disrupting bacterial membranes. This membrane disruption typically arises from nanoscale structural features such as sharp edges or protrusions, which physically puncture bacterial cell envelopes upon contact. The antibacterial efficacy of such MOFs is influenced by their morphological characteristics and surface charge distribution. Notably, negatively charged MOF surfaces can adsorb positively charged components of bacterial membranes *via* electrostatic interactions, leading to alterations in membrane potential and destabilization of integrity. He *et al.* constructed a three-dimensional hierarchical Cu-BDC MOF nanosheet array (Cu-BDC HS) using a two-step *in situ* growth method.[69] The nanosheets possess sharp, blade-like edges capable of directly penetrating bacterial membranes, resulting in intracellular content leakage (Fig. 7A). Meanwhile, the inter-nanosheet spacing is smaller than the average bacterial size, which impedes bacterial escape and enhances contact-based antimicrobial action. Antibacterial experiments showed that the inactivation efficiency of Cu-BDC HS against *S. aureus* and *E. coli* exceeded 99% within 60 min and maintained high efficiency after 5 consecutive antibacterial

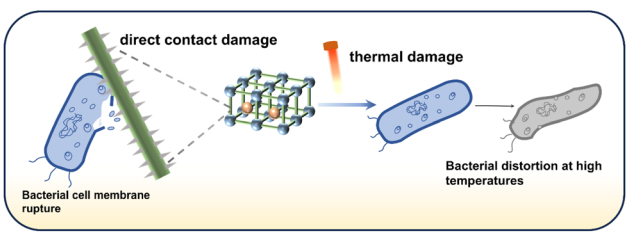

Fig. 6 Schematic diagram of the mechanism of physical stimulation based on MOFs for antibacterial applications.

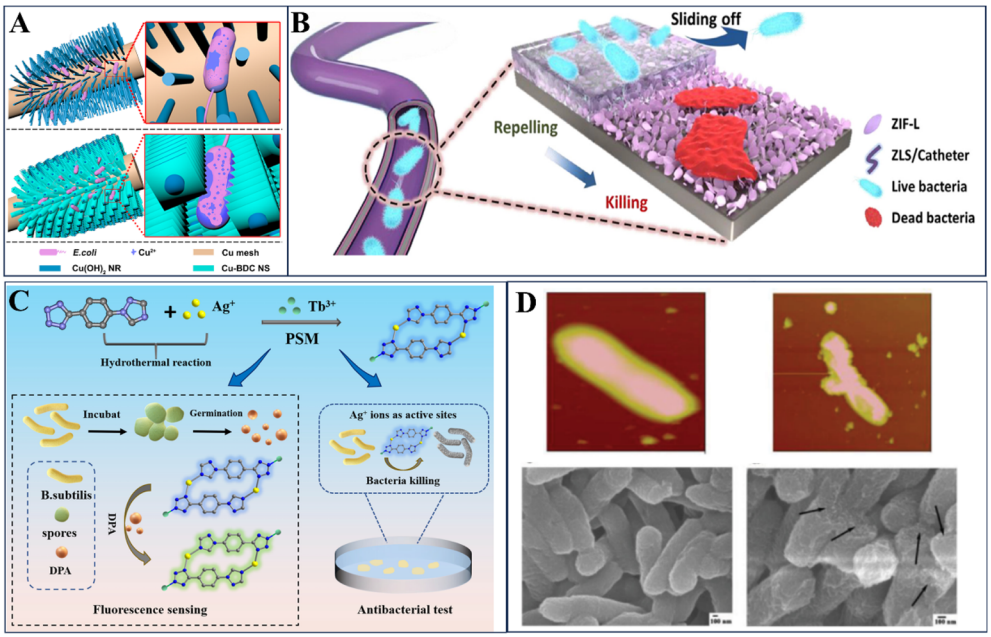

Fig. 7 MOFs destroys bacteria based on physical direct contact. (A) Cu – BDC MOF penetrates bacteria with its sharp edges (reprinted with permission from ref. 69 Copyright 2022, Elsevier). (B) Blade structure of ZIF-L pierces bacterial cell membrane (reprinted with permission from ref. 70 Copyright 2022, Elsevier). (C) Direct contact of the new Ag-MOF (Ag-tpt) leads to bacterial damage (Reprinted with permission from ref. 71 Copyright 2023, Elsevier). (D) ($Ag_{2n}(BTEC)_n/_2$) damages *E. coli* through direct contact (reprinted with permission from ref. 72 Copyright 2014, Wiley).

cycles. This synergistic effect of mechanical membrane disruption and sustained release of Cu^{2+} minimizes the cytotoxicity typically associated with high-concentration metal ions, while simultaneously offering prolonged antibacterial performance and favorable biocompatibility. In addition to nanoscale structural modifications of MOFs can be exploited for antibacterial purposes. Hao *et al.* designed a slippery liquid-infused porous surface (SLIPS) based on ZIF-L (Fig. 7B).[70] The infused lubricant layer serves as a non-fouling barrier that inhibits initial bacterial adhesion and biofilm formation. Importantly, in the event of mechanical wear or depletion of the lubricant, the underlying ZIF-L structure becomes exposed. This exposed layer possesses blade-like features capable of physically puncturing bacterial membranes, thereby providing a secondary antibacterial mechanism.

To mitigate the potential biological risks associated with the prolonged release of metal ions, Yin *et al.* designed a novel Ag-MOF, designated Ag-tpt, which exhibits high aqueous stability.[71] The antibacterial activity of Ag-tpt is attributed to its exposed active silver sites, which enable directly contact with bacteria (Fig. 7C). This direct-contact mechanism circumvents the cytotoxic effects typically associated with excessive Ag^+ ion release, thereby enhancing biocompatibility. Similarly, Li *et al.* designed a silver-based MOF, $Ag_{2n}(BTEC)_n/_2$, incorporating Ag^+ active centers capable of interacting with the outer membrane of *E. coli*.[72] Upon contact, this material disrupts bacterial homeostasis by altering intracellular Ca^{2+} and –SH balance, leading to destabilization and bacterial inactivation (Fig. 7D). Importantly, analysis using inductively coupled plasma-atomic emission spectrometry (ICP-AES) confirmed the absence of Ag^+ in both the extracellular solution and intracellular contents of *E. coli*, indicating that the antibacterial effect is independent of Ag^+ release and is instead mediated by surface-bound silver interactions.

The antibacterial effect of MOF through physical relies primarily on their intrinsic structural and physicochemical properties. The nanoscale dimensions of MOFs facilitate close interaction with bacteria, while their high specific surface area maximizes the extent of bacterial contact. Furthermore, the porous architecture of MOF can serve as a physical barrier, impeding bacterial proliferation and activity. These unique features position MOFs that operate *via* contact-mediated mechanisms as promising candidates for the development of next-generation antibacterial materials with reduced cytotoxicity and sustained efficacy.

2.3.2 Thermal damage. MOFs can also exert physical antibacterial effects through thermally induced mechanisms. One such mechanism involves volumetric expansion or contraction of MOF structures in response to temperature fluctuations. These structural transformations can generate localized mechanical pressure on bacterial cells, thereby compromising membrane integrity. Additionally, the high specific surface area and porous nature of MOFs facilitate the adsorption of bacterial cells onto their surfaces. Upon exposure to elevated temperatures, the bacteria in close contact with MOFs are subjected to direct thermal damage. Also, when heating occurs in aqueous environments, can lead to the generation of acoustic or pressure. These waves may induce physical rupture of bacterial membranes, contributing to the overall antibacterial effect. Despite these promising mechanisms, research focusing

exclusively on thermal damage induced by MOFs remains limited. In most studies, temperature-induced inactivation is accompanied by the generation of ROS, suggesting a synergistic bactericidal process. For example, Cheng *et al.* designed an $Mn_{0.1}$PCC composite material capable of generating heat under microwave irradiation (Fig. 8A).[73] This localized heating effect increased the permeability of bacterial membranes, while concurrently facilitating the production of substantial ROS levels under microwave exposure. The combined thermal and oxidative stress significantly enhanced the antibacterial performance of the material. Similarly, Pal *et al.* used MOFs as thermal catalysts to promote their efficient production of H_2O_2, thereby enhancing sterilization efficacy through temperature-induced processes (Fig. 8B).[74] These findings underscore the potential of MOF-based materials in employing thermal mechanisms, often in concert with ROS production, to achieve effective antibacterial outcomes.

In addition to chemical and structural properties, MOFs have demonstrated significant potential in photothermal antibacterial applications by converting absorbed light energy into thermal energy.[77] This process enhances antibacterial efficacy by generating localized high temperatures upon light irradiation. The primary mechanisms of photothermal antibacterial action include thermal-induced protein denaturation, which disrupts essential cellular components such as ribosomes and detoxifying enzymes, ultimately leading to cell inactivation and bacterial death.[78] Building upon this mechanism, numerous studies have explored the design of MOF-based composites that harness both photothermal and photodynamic effects for more efficient and versatile antibacterial performance. Cu-MOFs exhibit strong absorption in the NIR light region and effectively convert NIR light into heat. Upon irradiation, they induced rapid increases in their immediate environment, disrupting bacterial cells through thermal effects. Yu *et al.* synthesized a composite by integrating CuS NPs with HKUST-1, thereby achieving a dual-mode antibacterial strategy combining the photothermal and photodynamic effects (Fig. 8C).[75] Under NIR irradiation, the intrinsic d–d transitions of Cu^{2+} ions were activated, contributing to photothermal conversion. Additionally, CuS NPs, possessing intrinsic lattice defects and high concentrations of hole carriers, reacted with H_2O to produce ·OH. The ultimate antibacterial mechanisms are thermodynamically induced cell membrane disruption, protein denaturation, and photodynamic generation of ROS for DNA and enzyme destruction. A CuS content of 20% in the CuS/PCN composite yielded ~99% bacterial inactivation within 20 min of light exposure. However, excess CuS (>20%) led to charge recombination, reducing bactericidal efficiency. These results underscore the importance of optimizing composition, irradiation duration, and thermal output to maximize antibacterial performance while minimizing cytotoxicity.

In addition to Cu-based systems, other materials, such as Prussian blue (PB) also exhibit excellent photothermal properties due to the broad spectral absorption, particularly in the NIR region (650–900 nm). Luo *et al.* developed a heterojunction composite by combining PB with PCN-224 (Fig. 8D).[76] Under 660 nm light irradiation, type II band alignment between PB and PCN-224 facilitated efficient charge separation: photogenerated electrons in the conduction band (CB) of PB transferred to the CB of PCN-224, while valence band (VB) holes in PCN-224 moved to the VB of PB. This charge redistribution inhibited electron–hole recombination and enhanced $^1O_2$ generation, as a result, the composite achieved sterilization efficiencies of 99.84% for *S. aureus* and 99.3% for its biofilm within 15 min of irradiation. Photothermal effects have also been utilized in the synthesis of MOFs themselves. Shelonchik *et al.* introduced a strategy wherein the photothermal properties of plasmonic nanoparticles (PNPs) enabled localized high-temperature synthesis of MOFs under visible (520 nm) and NIR (660 and 850 nm) light.[79] This method allowed for the rapid synthesis of UiO-66 within 20 min under 850 nm LED illumination. Various MOFs including UiO-66, MIL-88A, HKUST-1, and MOF-5, were successfully synthesized using this technique, demonstrating compatibility with diverse photothermal materials such as gold nanospheres and carbon particles. Furthermore, a composite named AuBP@UiO-66 was fabricated, achieving photothermal conversion efficiencies high enough to reach temperatures of 250 °C within 5 min, presenting significant potential for antibacterial applications.

MOFs exhibit significant promise in photothermal and thermally synergistic antibacterial strategies. Their structural features allow for localized heating that can induce protein denaturation and membrane rupture, while concurrently enhancing ROS production. Under NIR light, MOFs are particularly effective in non-invasive, deep-tissue antibacterial applications. Numerous studies confirm that the antibacterial performance of MOFs in photothermal contexts can be optimized through rational material design, precise control of component ratios, and fine-tuning of irradiation parameters such as wavelength and duration. These thermally driven and photothermally synergistic mechanisms not only broaden the

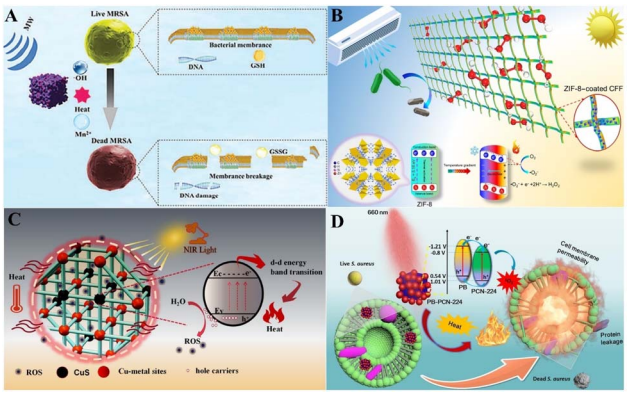

Fig. 8 MOFs destroy bacteria based on thermal damage. (A) $Mn_{0.1}$PCC generates heat for antibacterial (reprinted with permission from ref. 73 Copyright 2024, Wiley). (B) MOF produces H_2O_2 for antibacterial by temperature change (reprinted with permission from ref. 74 Copyright 2025, AAAS). (C) Cu-based MOF for antibacterial resistance under photothermal conditions (reprinted with permission from ref. 75 Copyright 2020, Elsevier). (D) PB and PCN-224 were combined and antibacterized under thermal damage at certain wavelengths (Reprinted with permission from ref. 76 Copyright 2021, Elsevier).

application scope of MOFs in antimicrobial contexts but also pave the way for the development of next-generation, high-efficiency, and controllable antibacterial materials.

3. Antibacterial applications of MOFs

Bacteria are broadly classified into Gram-positive and Gram-negative categories based on the structural characteristics of their cell walls. Gram-positive bacteria have a thick, multilayered peptidoglycan wall, a mesh-like polymer that provides mechanical strength and maintains cellular morphology. In contrast, Gram-negative bacteria feature a comparatively thinner peptidoglycan layer, located between the inner (cytoplasmic) membrane and an additional outer membrane. The outer membrane is rich in lipopolysaccharide (LPS), which contribute to the structural stability, pathogenicity, and immune evasion capabilities of Gram-negative bacteria (Fig. 9).[80] Due to these structural differences, Gram-positive bacteria are usually more susceptible to antibiotics that target the peptidoglycan layer. The outer membrane of Gram-negative bacteria acts as a formidable, limiting antibiotic penetration and rendering these bacteria more resistant to conventional treatments. Consequently, effective inactivation of Gram-negative bacteria often requires strategies capable of disrupting or circumventing this outer membrane barrier. In response to these challenges, recent research has focused on the rational design of MOF-based antibacterial agents with selective toxicity toward both Gram-positive and Gram-negative species. Tailoring the physicochemical properties of MOFs-such as pore size, surface charge, metal ion composition, and functional groups-enables targeted interaction with specific bacterial structures. As a result, researchers are increasingly developing MOFs with differential antibacterial mechanisms, thereby enhancing their applicability against a broad spectrum of bacterial pathogens based on their cell wall architecture.

3.1 Gram-positive bacteria

Given that peptidoglycan constitutes approximately 90% of the cell wall structure in Gram-positive bacteria, it represents a prime target for antibacterial intervention. Lysozyme, an enzyme capable of hydrolyzing the β-1,4-glycosidic bonds within peptidoglycan, has therefore been investigated in combination with MOFs to enhance antibacterial efficacy. Guan *et al.* designed a multifunctional nanozyme composite by immobilizing lysozyme on Fe_3O_4@PVP@NH_2-MIL-88B(Fe), which was further combined with the antimicrobial agent carvacrol to synthesize Fe_3O_4@PVP@MIL-88B(Fe)-NH-lysozyme/carvacrol (FPMLC). This hybrid material leverages electrostatic interactions to capture bacteria, employs infrared-triggered release of carvacrol to compromise bacterial membranes, and utilizes lysozyme to enzymatically degrade the bacterial cell wall (Table 1).[81]

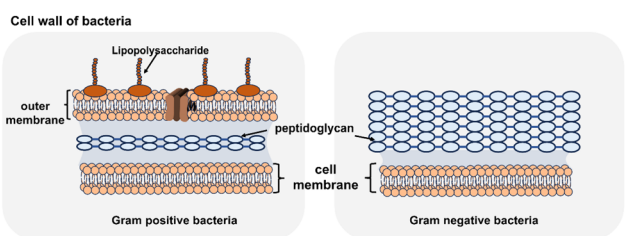

Fig. 9 Schematic representation of the cell walls of Gram-positive and Gram-negative bacteria.

The rapid proliferation of antibiotic-resistant bacteria has become a serious public health problem. Among Gram-positive antibiotic-resistant bacteria, MRSA, vancomycin-resistant enterococci (VRE), and multidrug-resistant *S. aureus* (MDRSA) are particularly prevalent. In response to this growing threat, researchers have been actively developing MOFs to enhance antimicrobial efficacy. Vancomycin, a commonly used antibiotic in clinical practice, has been instrumental in treating bacterial infections. However, its prolonged use has contributed to the emergence of vancomycin-resistant *S. aureus* (VRSA). The synergistic integration of vancomycin with other antimicrobial agents has been explored. Chowdhuri *et al.* developed a ZIF-8@FA@VAN to combat MDRSA. Their study demonstrated that neither VAN alone or ZIF-8@FA NMOFs exhibited significant antibacterial activity. But the ZIF-8@FA@VAN NMOFs showed pronounced antibacterial effects, highlighting the potential of MOF-based delivery systems in overcoming antibiotic resistance.[114] Zeolite imidazolate frameworks (ZIFs) are also capable of a range of combined therapeutic bactericidal by light accordingly. MRSA remains one of the most encountered antibiotic-resistant bacteria. To combat it, Song *et al.* designed a GOx-Fe_3O_4@MIL material, in which glucose oxidase (Gox) catalyzes the oxidation of glucose to gluconic acid and H_2O_2, while Fe_3O_4 exerts POD activity, generating ·OH for bacterial inactivation. Antibacterial test revealed a 94% inactivation rate of MRSA demonstrating the effectiveness of this cascade catalytic strategy.[115]

3.2 Gram-negative bacteria

The cell wall of Gram-negative bacteria is characterized by a relatively thin peptidoglycan and an outer membrane rich in phospholipids and LPS. This outer membrane serves as a formidable barrier, significantly enhancing resistance to antibiotic penetration. It has been found that Cu-MOFs have a more significant bactericidal effect on Gram-negative bacteria. The release of Cu^{2+} plays a central role in this activity, as these ions exhibit a strong affinity for LPS and membrane-associated proteins, leading to the disruption of the outer membrane integrity. In addition, Cu-MOFs possess intrinsic oxidase (OXD)-like activity, catalyzing the generation of $^1O_2$, which further contributes to their antibacterial properties.[116] Hsu *et al.* designed a guanine-coated Cu-MOF (Guanine-Cu-MOF) for the targeted eradication of *P. aeruginosa*. The primary antibacterial mechanism involved the release of Cu^{2+}, which electrostatically interacts with the negatively charged bacterial cell wall, penetrates the membrane and induces structural damage.[116] To further improve the antibacterial performance, Rodríguez. *et al.* immobilized MOF-199 onto cellulose fibers, creating

Table 1 Evaluation of antibacterial performance of different MOFs in Gram-positive bacteria

No.	MOFs	Type of bacteria	Antibacterial activity	Antibacterial mechanism	Ref.
1	$MnFe_2O_4$@MIL/Au&GOx	*S. aureus*	MIC = 31.2 μg mL^{-1}	Generate a large amount of ROS	82
2	BioMIL-5	*S. aureus*	MIC = 1.7 mg mL^{-1} MBC = 4.3 mg mL^{-1}	Zn^{2+} release, azelaic acid (AzA)	83
3	MOF-5	*S. aureus*	Inhibition zone diameter = 10 mm	Zn^{2+} release	84
4	PDMS@H-MOF-5	*S. aureus*	Inhibition zone diameter = 30 mm	Zn^{2+} release	85
5	Co (Hin) DMF	*S. aureus*	MIC = 6.25 μg mL^{-1}	Co^{2+} release	86
	O_2–Cu/ZIF-8@Ce_6/ZIF-8@HA	*S. aureus*	MIC = 50 μg mL^{-1}	Photodynamic therapy (PDT)	87
6	HuA@ZIF-8 NPs	*S. aureus*	Antibacterial efficiency = 99.59%	Photothermal therapy (PTT) and Zn^{2+} release	88
7	AuNR@ZIF-8@AuNCs	*S. aureus*	Antibacterial efficiency = 99%	Photodynamic therapy produces ROS	89
8	Prussian blue under microwave (55 °C)	*S. aureus*	Antibacterial efficiency = 99.08%	Produces ROS	90
9	CCM@ZIF-8@HA@CS	*S. aureus*	MIC = 0.625 μg mL^{-1}	Produces ROS	91
10	Au@ZIF-8	*S. aureus*	Antibacterial efficiency = 99.9%	Produces ROS	92
11	MIL-100@PMB@HA	*S. aureus*, MRSA	Antibacterial efficiency = 98.5% and 98.4%	·OH	93
12	PCN-224(Zr/Ti)	*S. aureus*, *S. epidermidis*, MRSA, MRSE	Antibacterial efficiency = 96.2%, 96.0%, 96.8% and 96.2%	Produces ROS	94
13	N–Cu-MOF@Cys/ MNP@PAMAM	*S. aureus*	Inhibition zone diameter = 14 mm	Cu^{2+} release	95
14	Cu_{10}MOF	*S. aureus*	Antibacterial efficiency = 99.71%	Synergetic action of photothermal and photocatalytic properties	96
15	Zn-Por-COPs	*S. aureus*	Antibacterial efficiency = 99.65%	Photodynamic generation of ROS	97
16	OH-Por-COPs	*S. aureus*	Antibacterial efficiency = 89.16%	Photodynamic generation of ROS	97
17	H_2-Por-COPs	*S. aureus*	Antibacterial efficiency = 81.77%	Photodynamic generation of ROS	97
18	Cruciform petal-like ZIF-8	*S. aureus*	MIC = 0.5 mg mL^{-1} MBC = 1 mg mL^{-1}	Photodynamic generation of ROS, release of active zinc compounds	98
19	PM/Ag–Ce_6@ZIF-8	*S. aureus*	MIC = 40 μg mL^{-1}	Zn^{2+} release and photodynamic generation of ROS	99
20	Cu–Zn-MOF-2	*S. aureus*, *B. subtilis*	Inhibition zone diameter = 4.0 ± 0.3 cm, 1.4 ± 0.1 cm	Produces ROS	100
21	MOF@Cu^{2+}	*S. aureus*	Antibacterial efficiency = 98.9%	Cu^{+} release and photodynamic generation of ROS	101
22	ZIF-67 HS	*S. aureus*	MIC = 6.25 μg mL^{-1}	Produces ROS	102
23	Ag@Cu-MOF@BG	*S. aureus*, *C. albicans*	MIC = 125 μg mL^{-1}, 125 μg mL^{-1}	Produces ROS	103
24	Ag@Gd-BBDC1.25	*S. aureus*	Survival percentage = 0.53 ± 0.05%	Produces ROS	104
25	Gelatin/Fe-PM@CD composite film	*S. aureus*	Inhibition zone diameter = 3.6 mm	Photodynamic generation of ROS	105
26	PVP@S-PCN-134	*S. aureus*	Antibacterial efficiency = 97.5%	Photodynamic generation of ROS	106
27	Ag@Ni-MOF	*S. pyogenes*, *S. epidermidis*, *C. albicans*	MIC = 2048 μg mL^{-1}, 4096 μg mL^{-1} and 2048 μg mL^{-1}	Ag^{+} release and produces ROS	107
28	ZG-Zn-MOF@Nio	*S. aureus*, *B. subtilis*	Inhibition Zone = 22 ± 1.21 mm, 20 ± 0.41 mm. MIC = 31.25 μg mL^{-1}, 31.25 μg mL^{-1}	—	108
29	Bi NPs/PCN-224	*S. aureus*, *MRSA*	Antibacterial efficiency = 98.3%, 98.6%	Bi^{3+} release and produces ROS	109
30	(Cu/DPA-MOF/OP/CS) hydrogel polymer	*L. monocytogenes*, *S. epidermidis*, *B. cereus*, *C. equi*, *S. aureus*	MIC = 64 μg mL^{-1}, 4 μg mL^{-1}, 64 μg mL^{-1}, 32 μg mL^{-1} and 1 μg mL^{-1}	—	110
31	Cu/Co-hybrid MOF/PVA	*B. cereus*, *S. aureus*, *S. pyogenes*	MIC = 16 μg mL^{-1}, 64 μg mL^{-1} and 16 μg mL^{-1}	—	111
32	Ag NPs@ACM-1	*S. aureus*, MRSA	MBC = 39.1 μg mL^{-1}, 62.5 μg mL^{-1}	Photodynamic generation of ROS	112
33	Ce_6@MOF-Gel	*S. aureus*	MIC = 0.38 mg mL^{-1}	Zn^{2+} release and ROS generated under laser	113

Table 2 Evaluation of antibacterial performance of different MOFs in Gram-negative bacteria

No.	MOFs	Type of bacteria	Antibacterial activity	Antibacterial mechanism	Ref.
1	Ni-MOFs	*P. aeruginosa*	MIC = 1000 μg mL^{-1}	Ni^{2+} release	121
2	UiO-66-2COOAg	*E. coli*	MIC = 75 μg mL^{-1}	Ag^{+} release	122
3	Chlorhexidine-Cu-BTC	*E. coli*	Inhibition zones = 22 mm	Cu^{2+} release	123
4	Bi_2S_3/FeS_2	*E. coli*	Antibacterial efficiency reached more than 99.9%	·OH	124
5	Fe_3O_4@MOF@Au NP	*E. coli*	The inhibition rate can be greater than 99%	·OH	125
6	HKUST-Hs	*E. coli*	The growth inhibition of more than 98%	Cu^{2+} release	126
7	Zn-MOF	*P. aeruginosa*	MIC = 0.08 mg mL^{-1} MBC = 2.56 mg mL^{-1}	Zn^{2+} release	127
8	MIL-101(Fe)@ZnO	*P. aeruginosa*	The inhibition rate can reach 92.71%	Zn^{2+} and Fe^{2+} release; generate a large amount of ROS	128
9	ZIF-8@SnO_2@CoFe2O4	*E. coli*	Inhibition zones = 18 mm	Ni^{2+} release	129
10	MIL-100(Fe)NPs-gentamicin	*P. aeruginosa*	MIC = 1–2 mg L^{-1} MBC = 4–8 mg L^{-1}	Produces ROS	130
11	CA@Ag@CD-MOF/PDMS	*E. coli*	MIC = 0.25 mg L^{-1} MBC = 0.25 mg L^{-1}	Release of caffeic acid (CA) and Ag^{+}	131
12	MIL-100@PMB@HA	*E. coli*	Antibacterial efficiency = 100%	·OH	93
13	PCN-224(Zr/Ti)	MDR *E. coli*, *E. coli*, MDR *A. baumannii*, *A. baumannii*	Antibacterial efficiency = 96.4%, 98.8%, 100% and 100%	Produces ROS	94
14	N–Cu-MOF@Cys/MNP@PAMAM	*E. coli*	Inhibition zones = 11 mm	Cu^{2+} release	95
15	Cu_{10}MOF	*E. coli*	Antibacterial efficiency = 97.14%	Synergetic action of photothermal and photocatalytic properties	96
16	Zn-Por-COPs	*E. coli*	Antibacterial efficiency = 97.25%	Photodynamic generation of ROS	97
17	OH-Por-COPs	*E. coli*	Antibacterial efficiency = 86.15%	Photodynamic generation of ROS	97
18	H_2-Por-COPs	*E. coli*	Antibacterial efficiency = 79.15%	Photodynamic generation of ROS	97
19	LBA-AmX-Zn-MOFs	*H. pylori*	MIC = 10 μg mL^{-1}	Drug release	132
20	Cruciform Petal-like ZIF-8	*E. coli*	MIC = 0.5 mg mL^{-1} MBC = 0.5 mg mL^{-1}	Photodynamic generation of ROS, release of active zinc compounds	98
21	PM/Ag–Ce_6@ZIF-8	*E. coli*	MIC = 60 μg mL^{-1}	Zn^{2+} and photodynamic generation of ROS	99
22	Cu–Zn-MOF-2	*E. coli*	Inhibition zones = 4.5 ± 0.2 cm	Produces ROS	100
23	Ag@Cu-MOF@BG	*E. coli*, *K. pneumoniae*, *P. aeruginosa*	MIC = 62.5 μg mL^{-1}, 62.5 μg mL^{-1} and 31.125 μg mL^{-1}	Produces ROS	103
24	Ag@Gd-BBDC1.25	*E. coli*	Survival percentage = 30 ± 0.89%	Produces ROS	104
25	Gelatin/Fe-PM@CD composite film	*E. coli*	Inhibition zone diameter = 2.9 mm	Photodynamic generation of ROS	105
26	Ag@Ni-MOF	*E. coli*, *P. aeruginosa*, *K. pneumoniae*, *A. baumannii*	MIC = 2048 μg mL^{-1}, 128 μg mL^{-1}, 512 μg mL^{-1}, 2048 μg mL^{-1}	Ag^{+} and generation of ROS	107
27	ZG-Zn-MOF@Nio	*E. coli*, *P. aeruginosa*	Inhibition Zone = 16 ± 0.89 mm, 18 ± 0.48 mm. MIC = 62.5 μg mL^{-1}, 62.5 μg mL^{-1}	—	108
28	Bi NPs/PCN-224	*E. coli*	Antibacterial efficiency = 99.1%	Bi^{3+} and generation of ROS	109

Table 2 (*Contd.*)

No.	MOFs	Type of bacteria	Antibacterial activity	Antibacterial mechanism	Ref.
29	(Cu/DPA-MOF/OP/CS) hydrogel polymer	*K. pneumoniae*, *E. coli*, *Y. enterocolitica*, *P. mirabilis*, *A. baumannii*	MIC = 4 μg mL^{-1}, 64 μg mL^{-1}, 32 μg mL^{-1}, 32 μg mL^{-1} and 64 μg mL^{-1}	—	110
30	Cu/Co-hybrid MOF/PVA	*P. mirabilis*, *E. coli*	MIC = 64 μg mL^{-1}, 256 μg mL^{-1}	—	111
31	Ag NPs@ACM-1	*E. coli*	MBC = 39.1 μg mL^{-1}	Photodynamic generation of ROS	112
32	AgBDC MOF	*E. coli*	MIC = 100–200 ppm	Ag^{+} and generation of ROS	133

a composite (Cellulose-MOF-199) that was tested against *E. coli*. Quantitative test revealed a decrease in bacterial concentration from an initial 16 000 ± 3.7 CFU mL^{-1} to 0 CFU mL^{-1}.[117] Although some of this reduction may be attributed to mechanical stress or cell adhesion during the soaking process, qualitative assessments confirmed the composite's inherent antibacterial activity and its potential for broad-spectrum antimicrobial applications.

The escalating prevalence of multidrug-resistant bacteria poses serious challenges to global health, contributing to more complicated treatment protocols, increased healthcare expenditures, and elevated mortality rates. The most critical drug-resistant bacteria include *Acinetobacter baumannii* (*A. baumannii*, carbapenem), *P. aeruginosa* (carbapenem), Enterobacteriaceae, extended-spectrum β-lactamase-producing (carbapenem), *Enterococcus faecalis* (*E. faecalis*, vancomycin), *S. aureus* (methicillin, vancomycin), *Helicobacter pylori* (*H. pylori*, clarithromycin), *Campylobacter* spp. (fluoroquinolone), *Salmonellae* (fluoroquinolone), *Neisseria gonorrhoeae* (cephalosporin, fluoroquinolone), *Streptococcus pneumoniae* (penicillin-non-susceptible), *Haemophilus influenzae* (ampicillin), *Shigella* spp. (fluoroquinolone).[118] To counter these threats, there is a pressing need to develop novel and more effective antibacterial agents.[119] For the first-ranked carbapenem-resistant, *A. baumannii* is a Gram-negative bacillus that causes serious infections, however, it is resistant to carbapenem antibiotics, In response, Hou *et al.* developed a bimetallic PCN-224 (Zr/Ti) material capable of producing ROS under light irradiation, achieving significant reduction in *A. baumannii* viability after just 10 min exposure.[94] Furthermore, Niu *et al.* synthesized a pH-responsive nanodelivery system by loading negatively charged imipenem onto ZIF-8 nanoparticles. This system not only facilitated controlled drug release but also generated ROS to enhance antibacterial effects, offering a promising approach for combating carbapenem-resistant *A. baumannii*.[120] Such strategies, which integrate antibiotics with MOF-based nanomaterials, represent a cutting-edge direction in the development of therapeutic interventions targeting Gram-negative bacterial resistance (Table 2).

4. Conclusion and prospects

This review categorizes the antibacterial mechanisms of MOFs into three primary classes: (1) release of metal ions, (2) ROS generation (*via* metal centers, ligands, and metal center–ligand interactions), and (3) physical stimuli (direct contact, thermal stimulation). Furthermore, it provides a comparative analysis of the antibacterial efficacy among various MOF systems and outlines modification strategies aimed at enhancing their antimicrobial performance. The review also addresses the favorable biocompatibility of MOFs. Finally, it consolidates information on the antibacterial efficiency and specific mechanisms of MOFs against both Gram-positive and negative bacteria.

Despite their promising antibacterial properties, several challenges hinder the practical application of MOFs. These include thermal instability, limited bacterial selectivity, and

concerns over long-term biocompatibility and environmental persistence. Future efforts should focus on designing low-cost, thermally stable, and biodegradable MOFs with high selectivity for target pathogens. Strategies such as using biocompatible metals and degradable ligands are particularly promising for improving safety and reducing ecological risks.

In conclusion, advancing the design of MOFs with enhanced antibacterial efficacy, stability, selectivity, and biodegradability will be critical for their safe and sustainable application in medicine, agriculture, and environmental remediation.

Data availability

No primary research results, software, or code have been included, and no new data were generated or analyzed as part of this review.

Author contributions

Yuan Tian: conceptualization, validation, writing – original draft, writing – review & editing. Bin Wang: methodology, formal analysis. Zerun Zhang: investigation. Tianhan Kai: software, funding acquisition. Pian Wu: supervision, writing – review & editing, funding acquisition. Ping Ding: supervision, project administration, funding acquisition.

Conflicts of interest

The authors declare that they have no known competing financial interests or personal relationships that could have appeared to influence the work reported in this paper.

Acknowledgements

This work was supported by the National Natural Science Foundation of China (grant number 82373635), the Natural Science Foundation of Hunan (grant number 2025JJ60624), the Natural Science Foundation of Changsha (grant number kq2402240), the Science and Technology Innovation Program of Hunan Province (Grant No. 2022RC1206).

References

1 K. S. Ikuta, L. R. Swetschinski, G. R. Aguilar, F. Sharara, T. Mestrovic, A. P. Gray, N. D. Weaver, E. E. Wool, C. Han and A. G. Hayoon, *Lancet*, 2022, **400**, 2221–2248.
2 J. Parsonnet, *Environ. Health Perspect.*, 1995, **103**, 263–268.
3 S. B. Levy and B. Marshall, *Nat. Med.*, 2004, **10**, S122–S129.
4 S. J. Dunachie, N. P. Day and C. Dolecek, *Curr. Opin. Microbiol.*, 2020, **57**, 95–101.
5 S. Jia, Y. Zhao, J. Liu, R. Qi, H. Liang and H. Yuan, *ACS Appl. Bio Mater.*, 2023, **6**, 3842–3847.
6 L. Qiu, C. Wang, M. Lan, Q. Guo, X. Du, S. Zhou, P. Cui, T. Hong, P. Jiang, J. Wang and J. Xia, *ACS Appl. Bio Mater.*, 2021, **4**, 3124–3132.
7 X. Chen, L. Wang, J. Sun, G. Wu, Z. Zhang, Q. Yu, W. Wang and M. Liu, *ACS Appl. Bio Mater.*, 2021, **4**, 5661–5668.
8 J. Du, Y. Cong, X. Wang, Y. Kang, P. Zhang and L. Li, *ACS Appl. Bio Mater.*, 2023, **6**, 3919–3926.
9 W. Gao, S. Thamphiwatana, P. Angsantikul and L. Zhang, *Wiley Interdiscip. Rev. Nanomed. Nanobiotechnol.*, 2014, **6**, 532–547.
10 A. Dumbrava, D. Berger, C. Matei, G. Prodan, F. Aonofriesei, M. D. Radu and F. Moscalu, *J. Inorg. Organomet. Polym. Mater.*, 2019, **29**, 2072–2082.
11 S. Shakya, Y. He, X. Ren, T. Guo, A. Maharjan, T. Luo, T. Wang, R. Dhakhwa, B. Regmi, H. Li, R. Gref and J. Zhang, *Small*, 2019, **15**, 1901065.
12 G. Xu, T. Yamada, K. Otsubo, S. Sakaida and H. Kitagawa, *J. Am. Chem. Soc.*, 2012, **134**, 16524–16527.
13 S. Chuhadiya, D. Suthar, S. Patel and M. Dhaka, *Coord. Chem. Rev.*, 2021, **446**, 214115.
14 P. Z. Moghadam, A. Li, S. B. Wiggin, A. Tao, A. G. P. Maloney, P. A. Wood, S. C. Ward and D. Fairen-Jimenez, *Chem. Mater.*, 2017, **29**, 2618–2625.
15 S. Abednatanzi, P. G. Derakhshandeh, H. Depauw, F.-X. Coudert, H. Vrielinck, P. Van Der Voort and K. Leus, *Chem. Soc. Rev.*, 2019, **48**, 2535–2565.
16 Z. Wang and S. M. Cohen, *Chem. Soc. Rev.*, 2009, **38**, 1315–1329.
17 L. Jiao, J. Y. R. Seow, W. S. Skinner, Z. U. Wang and H.-L. Jiang, *Mater. Today*, 2019, **27**, 43–68.
18 Q.-L. Zhu and Q. Xu, *Chem. Soc. Rev.*, 2014, **43**, 5468–5512.
19 K. L. Haas and K. J. Franz, *Chem. Rev.*, 2009, **109**, 4921–4960.
20 S. Mittapally, R. Taranum and S. Parveen, *J. Drug Deliv. Therapeut.*, 2018, **8**, 411–419.
21 C.-N. Lok, C.-M. Ho, R. Chen, Q.-Y. He, W.-Y. Yu, H. Sun, P. K.-H. Tam, J.-F. Chiu and C.-M. Che, *JBIC, J. Biol. Inorg. Chem.*, 2007, **12**, 527–534.
22 Z. Liu, Y. Wang, Y. Zu, Y. Fu, N. Li, N. Guo, R. Liu and Y. Zhang, *Mater. Sci. Eng., C*, 2014, **42**, 31–37.
23 B.-P. Xie, J.-W. Chai, C. Fan, J.-H. Ouyang, W.-J. Duan, B. Sun, J. Chen, L.-X. Yuan, X.-Q. Xu and J.-X. Chen, *ACS Appl. Bio Mater.*, 2020, **3**, 8525–8531.
24 Y. Yang, X. Wu, C. He, J. Huang, S. Yin, M. Zhou, L. Ma, W. Zhao, L. Qiu and C. Cheng, *ACS Appl. Mater. Interfaces*, 2020, **12**, 13698–13708.
25 X. Lu, J. Ye, D. Zhang, R. Xie, R. F. Bogale, Y. Sun, L. Zhao, Q. Zhao and G. Ning, *J. Inorg. Biochem.*, 2014, **138**, 114–121.
26 G. Ximing, G. Bin, W. Yuanlin and G. Shuanghong, *Mater. Sci. Eng., C*, 2017, **80**, 698–707.
27 A. Rauf, A. A. Khawaja, M. Javed, S. Mahmood, S. Iqbal, S. Nadeem, M. Jahangir, M. Ahmad, A. Bahadur and M. Alshalwi, *Inorg. Chem. Commun.*, 2024, **159**, 111802.
28 H. N. Abdelhamid and G. A. E. Mahmoud, *Appl. Organomet. Chem.*, 2023, **37**, e7011.
29 C. E. Santo, D. Quaranta and G. Grass, *Microbiologyopen*, 2012, **1**, 46–52.
30 A. Casey, D. Adams, T. Karpanen, P. Lambert, B. Cookson, P. Nightingale, L. Miruszenko, R. Shillam, P. Christian and T. Elliott, *J. Hosp. Infect.*, 2010, **74**, 72–77.
31 J.-E. Cun, X. Fan, Q. Pan, W. Gao, K. Luo, B. He and Y. Pu, *Adv. Colloid Interface Sci.*, 2022, **305**, 102686.

32 C. Guo, F. Cheng, G. Liang, S. Zhang, Q. Jia, L. He, S. Duan, Y. Fu, Z. Zhang and M. Du, *Chem. Eng. J.*, 2022, **435**, 134915.
33 H. Zheng, D. Wang, X. Sun, S. Jiang, Y. Liu, D. Zhang and L. Zhang, *Chem. Eng. J.*, 2021, **411**, 128524.
34 Y. Xiao, J. Jiang, R. Cai, J. Fu, S. Xiang, S. Zhao, F. Fu, H. Diao and X. Liu, *Adv. Fiber Mater.*, 2024, **6**, 444–457.
35 C. Yuan, Y. Miao, Y. Chai, X. Zhang, X. Dong and Y. Zhao, *Molecules*, 2023, **28**, 6662.
36 S. Yao, J. Chi, Y. Wang, Y. Zhao, Y. Luo and Y. Wang, *Adv. Healthcare Mater.*, 2021, **10**, 2100056.
37 F.-Y. Kang, Y.-J. Su, X.-Z. Huang, Z.-L. Zhao and F.-Q. Liu, *J. Cent. S. Univ.*, 2023, **30**, 3237–3247.
38 J. Xu, Z. Ding, M. Wang, G. Wu and J. Xie, *Small*, 2024, **20**, 2406171.
39 L. Xie, H. Yang, X. Wu, L. Wang, B. Zhu, Y. Tang, M. Bai, L. Li, C. Cheng and T. Ma, *Biosafety and Health*, 2022, **04**, 135–146.
40 P. Prachi, A. Archana, M. Prajapati, S. Rai, P. R. Solanki and C. R. Kant, *Biologia*, 2025, **80**, 2133–2144.
41 V. B. Borisov, S. A. Siletsky, M. R. Nastasi and E. Forte, *Antioxidants*, 2021, **10**, 839.
42 Y. Hong, J. Zeng, X. Wang, K. Drlica and X. Zhao, *Proc. Natl. Acad. Sci. U. S. A.*, 2019, **116**, 10064–10071.
43 L. Wang, C. Hu and L. Shao, *Int. J. Nanomed.*, 2017, 1227–1249.
44 J. M. V. Makabenta, A. Nabawy, C.-H. Li, S. Schmidt-Malan, R. Patel and V. M. Rotello, *Nat. Rev. Microbiol.*, 2021, **19**, 23–36.
45 W. Huang, H. Yuan, H. Yang, Y. Shen, L. Guo, N. Zhong, T. Wu, Y. Shen, G. Chen and S. Huang, *Adv. Sci.*, 2025, **12**, 2410703.
46 Z. Li, C.-J. Xie, X.-W. Ren, Q. Zhang and B.-J. Ma, *Rare Met.*, 2023, **42**, 1899–1911.
47 Z. Wang, W. Guo, K. Zhang, Y. Ye, Y. Wang, D. Sui, N. Zhao and F.-J. Xu, *Sci. China Technol. Sci.*, 2022, **65**, 1052–1058.
48 S. Peng, R. Li, Y. Rao, Y. Huang, Y. Zhao, M. Xiong, J. Cao and S. Lee, *Appl. Catal., B*, 2022, **316**, 121693.
49 L. Lai, W. Zou, Y. Zhang, Y. Tu, S. Li, T. Xin, T. Zhou, S. Xu, P. Zheng, Q. Pan and W. Zhu, *Chem. Eng. J.*, 2022, **435**, 135084.
50 L. Hao, R. Jiang, Y. Fan, J.-n. Xu, L. Tian, J. Zhao, W. Ming and L. Ren, *ACS Sustain. Chem. Eng.*, 2020, **8**, 15834–15842.
51 M. Wang, L. Nian, Y. Cheng, B. Yuan, S. Cheng and C. Cao, *Chem. Eng. J.*, 2021, **426**, 130832.
52 J. Guo, H. Ma, H. Shang, W. Wang, R. Yang, S. Wang, Y. Miao, D. L. Phillips, G. Li and S. Xiao, *J. Hazard. Mater.*, 2025, **492**, 138060.
53 K. Liu, Y. Gao, J. Liu, Y. Wen, Y. Zhao, K. Zhang and G. Yu, *Environ. Sci. Technol.*, 2016, **50**, 3634–3640.
54 J. Wen, X. Liu, L. Liu, X. Ma, A. Fakhri and V. K. Gupta, *Colloids Surf., A*, 2021, **610**, 125683.
55 D. Wang, L. Niu, Z.-Y. Qiao, D.-B. Cheng, J. Wang, Y. Zhong, F. Bai, H. Wang and H. Fan, *ACS Nano*, 2018, **12**, 3796–3803.
56 X. Liang, X. Li, X. Yue and Z. Dai, *Angew. Chem., Int. Ed.*, 2011, **50**, 11622–11627.
57 C. Tang, X. Li, Y. Hu, X. Du, S. Wang, B. Chen and S. Wang, *Molecules*, 2024, **29**, 467.
58 W. Zhou, S. Begum, Z. Wang, P. Krolla, D. Wagner, S. Bräse, C. Wöll and M. Tsotsalas, *ACS Appl. Mater. Interfaces*, 2018, **10**, 1528–1533.
59 S. Elmehrath, K. Ahsan, N. Munawar, A. Alzamly, H. L. Nguyen and Y. Greish, *RSC Adv.*, 2024, **14**, 15821–15831.
60 M. Zhou, B. Zhang, T. Wang, P. Xiao, L. Cheng and R. Tang, *Mater. Adv.*, 2024, **5**, 7035–7039.
61 K. Wu, X.-Y. Liu, P.-W. Cheng, Y.-L. Huang, J. Zheng, M. Xie, W. Lu and D. Li, *J. Am. Chem. Soc.*, 2023, **145**, 18931–18938.
62 Y.-B. Huang, J. Liang, X.-S. Wang and R. Cao, *Chem. Soc. Rev.*, 2017, **46**, 126–157.
63 J. Wang, S. P. Teong, S. N. Riduan, A. Armugam, H. Lu, S. Gao, Y. K. Yean, J. Y. Ying and Y. Zhang, *J. Am. Chem. Soc.*, 2024, **146**, 599–608.
64 J. Wang, Y. Wang, D. Zhang, W. Ren and Z. Yang, *J. Colloid Interface Sci.*, 2022, **623**, 182–195.
65 Z. X. Yang, C. H. Chen, B. Li, Y. F. Zheng, X. M. Liu, J. Shen, Y. Zhang and S. L. Wu, *Chem. Eng. J.*, 2023, **451**, 139127.
66 D. Bagchi, A. Bhattacharya, T. Dutta, S. Nag, D. Wulferding, P. Lemmens and S. K. Pal, *ACS Appl. Bio Mater.*, 2019, **2**, 1772–1780.
67 K. Huang, F. P. Li, K. Yuan, Y. Q. Yang, H. S. Chang, Y. K. Liang, X. Z. Yan, J. Zhao, T. T. Tang and S. B. Yang, *Appl. Mater. Today*, 2022, **28**, 101513.
68 X. Cheng, H. Ma, R. Yang, H. Zhang, W. Wang, Y. Miao and S. Xiao, *ACS Sustain. Chem. Eng.*, 2025, **13**, 4252–4264.
69 C. H. He, C. Liu, M. Y. Li, M. Li, J. L. Yin, S. M. Han, J. Xia, D. Y. Chen, W. B. Cao, Q. P. Lu and F. Rosei, *Chem. Eng. J.*, 2022, **446**, 137381.
70 L. W. Hao, R. J. Jiang, J. Gao, J. N. Xu, L. M. Tian, X. Zhang, S. Z. Zhou, J. Zhao and L. Q. Ren, *Appl. Mater. Today*, 2022, **27**, 101430.
71 Y. Y. Yin, J. Zhang, R. Q. Fan, K. Zhu, X. Jiang, C. S. Ji, W. W. Jia, J. K. Wu, H. Tao and Y. L. Yang, *J. Hazard Mater.*, 2023, **446**, 130753.
72 W. Li, S. Zhou, S. Gao, S. Chen, M. Huang and R. Cao, *Adv. Mater. Interfaces*, 2015, **2**, 1400405.
73 H. Cheng, Y. Q. Yang, Y. Y. Wang, J. Q. Guo, X. Jiao, D. Huang, M. W. An, X. H. Yao, P. K. Chu and X. Y. Zhang, *Adv. Funct. Mater.*, 2024, **34**, 2405421.
74 A. Pal, S. Suresh, A. Khan, L. H. Kuo, L. T. Chi, A. Ganguly, C. Y. Kao, M. K. Sharma, T. S. A. Wang, D. Y. Kang and Z. H. Lin, *Sci. Adv.*, 2025, **11**, eads4711.
75 P. L. Yu, Y. J. Han, D. L. Han, X. M. Liu, Y. Q. Liang, Z. Y. Li, S. L. Zhu and S. L. Wu, *J. Hazard Mater.*, 2020, **390**, 122126.
76 Y. Luo, X. M. Liu, L. Tan, Z. Y. Li, K. W. K. Yeung, Y. F. Zheng, Z. D. Cui, Y. Q. Liang, S. L. Zhu, C. Y. Li, X. B. Wang and S. L. Wu, *Chem. Eng. J.*, 2021, **405**, 126730.
77 H. G. Jin, P. C. Zhao, Y. Y. Qian, J. D. Xiao, Z. S. Chao and H. L. Jiang, *Chem. Soc. Rev.*, 2024, **53**, 9378–9418.
78 C. D. Momo, Y. Zhou, L. X. Li, W. S. Zhu, L. Y. Wang, X. P. Liu, W. Bing and Z. J. Zhang, *Front. Chem.*, 2022, **10**, 1044931.
79 O. Shelonchik, N. Lemcoff, R. Shimoni, A. Biswas, E. Yehezkel, D. Yesodi, I. Hod and Y. Weizmann, *Nat. Commun.*, 2024, **15**, 1154.

80 W. W. Navarre and O. Schneewind, *Microbiol. Mol. Biol. Rev.*, 1999, **63**, 174.
81 W. Q. Nong, Y. L. Chen, D. Y. Lv, Y. T. Yan, X. Zheng, X. M. Shi, Z. Xu, W. L. Guan, J. Wu and Y. G. Guan, *Chem. Eng. J.*, 2022, **431**, 134003.
82 X. Zhou, S. Zhang, Y. Liu, J. S. Meng, M. X. Wang, Y. J. Sun, L. B. Xia, Z. Z. He, W. X. Hu, L. Ren, Z. W. Chen and X. C. Zhang, *ACS Appl. Mater. Interfaces*, 2022, **14**, 11104–11115.
83 C. Tamames-Tabar, E. Imbuluzqueta, N. Guillou, C. Serre, S. R. Miller, E. Elkaïm, P. Horcajada and M. J. Blanco-Prieto, *CrystEngComm*, 2015, **17**, 456–462.
84 M. Nakhaei, K. Akhbari, M. Kalati and A. Phuruangrat, *Inorg. Chim. Acta.*, 2021, **522**, 120353.
85 S. Barthwal, Y. Jeon and S. H. Lim, *Sustain. Mater. Technol.*, 2022, **33**, e00492.
86 L. W. Zhu, N. Liu, L. M. Yu, X. H. Jiang and X. Li, *Inorg. Chim. Acta.*, 2020, **510**, 119728.
87 R. F. Wang, Q. Y. Pan, F. Li, J. Y. Guo, Y. R. Huo, C. Xu, M. W. Xiong, Z. Y. Cheng, M. Liu and J. Lin, *Dalton Trans.*, 2023, **52**, 16189–16196.
88 Z. W. Liu, L. Tan, X. M. Liu, Y. Q. Liang, Y. F. Zheng, K. W. K. Yeung, Z. D. Cui, S. L. Zhu, Z. Y. Li and S. L. Wu, *Colloids Surf., B*, 2020, **188**, 110781.
89 W. F. Guo, W. X. Gao, Q. Li, S. H. Qu, L. B. Zhang, L. L. Tan and L. Shang, *J. Mater. Chem. A*, 2023, **11**, 2391–2401.
90 S. B. Wei, Y. Q. Qiao, Z. C. Wu, X. M. Liu, Y. Li, Z. D. Cui, C. Y. Li, Y. F. Zheng, Y. Q. Liang, Z. Y. Li, S. L. Zhu, H. R. Wang, X. B. Wang, R. C. Che and S. L. Wu, *Nano Today*, 2021, **37**, 101090.
91 S. H. Duan, X. Zhao, Z. H. Su, C. Wang and Y. Lin, *ACS Appl. Bio Mater.*, 2020, **3**(6), 3673–3680.
92 Z. W. Deng, M. H. Li, Y. Hu, Y. He, B. L. Tao, Z. Yuan, R. Wang, M. W. Chen, Z. Luo and K. Y. Cai, *Chem. Eng. J.*, 2021, **420**, 129668.
93 L. Guo, Y. X. Tang, L. Wang, R. Zhou, S. Y. Wang, H. Q. Xu, X. Yang, J. Z. Zhang, J. Chen, C. N. Xu, Y. H. Li and H. Y. Tian, *Adv. Funct. Mater.*, 2024, **34**, 2403188.
94 M. Chen, Z. Long, R. H. Dong, L. Wang, J. J. Zhang, S. X. Li, X. H. Zhao, X. D. Hou, H. W. Shao and X. Y. Jiang, *Small*, 2020, **16**, 1906240.
95 S. Asgari, G. M. Ziarani, A. Badiei, M. Rostami and M. Kiani, *Mater. Today Commun.*, 2022, **33**, 104393.
96 D. L. Han, Y. J. Han, J. Li, X. M. Liu, K. W. K. Yeung, Y. F. Zheng, Z. D. Cui, X. J. Yang, Y. Q. Liang, Z. Y. Li, S. L. Zhu, X. B. Yuan, X. B. Feng, C. Yang and S. L. Wu, *Appl. Catal., B*, 2020, **261**, 118248.
97 Q. B. Fu, X. Sun, T. T. Zhang, J. Pei, Y. J. Li, Q. B. Li, S. K. Zhang, G. I. N. Waterhouse, H. S. Li and S. Y. Ai, *Sci. Total Environ.*, 2024, **906**, 167475.
98 B. W. Shen, Y. X. Wang, X. L. Wang, F. E. Amal, L. Y. Zhu and L. Jiang, *Int. J. Mol. Sci.*, 2022, **23**, 7510.
99 L. Chen, Y. Wang, X. Huang, L. Han, Z. Huang, L. Guo, K. Chen and G. Tan, *J. Controlled Release*, 2025, **380**, 1164–1183.
100 A. R. Krithikka, D. Pushparani and D. Santhanaraj, *Inorg. Chem. Commun.*, 2025, **176**, 114194.
101 Y. Zhang, L. Li, H. Liu, H. Zhang, M. Wei, J. Zhang, Y. Yang, M. Wu, Z. Chen and C. Liu, *J. Mater. Chem. B*, 2024, **12**, 1317–1329.
102 Q. Zhang, R. Liu, S. Yan, X. Yan and Y. Lv, *Chem. Mater.*, 2025, **37**, 2204–2219.
103 M. Fandzloch, A. W. Augustyniak, J. Trzcińska-Wencel, P. Golińska and K. Roszek, *Dalton Trans.*, 2024, **53**, 10928–10937.
104 Y. Yu, T. Cui, C. Liu, W. Yang and B. Zhang, *Adv. Sci.*, 2025, **12**, 2415209.
105 P. Ananthi, N. R. V, H. K, P. A and A. Pius, *ACS Sustain. Chem. Eng.*, 2025, **13**, 3052–3065.
106 B. Xue, X. Geng, H. Cui, H. Chen, Z. Wu, H. Chen, H. Li, Z. Zhou, M. Zhao, C. Tan and J. Li, *Chin. Chem. Lett.*, 2023, **34**, 108140.
107 A. Mirshekar, P. Ghamari kargar, G. Bagherzade and H. Beyzaei, *Inorg. Chem. Commun.*, 2024, **164**, 112455.
108 H. M. Alharbi, A.-N. M. A. Alaghaz, T. A. Al Hujran, Z. E. Eldin and S. Elbeltagi, *Mater. Today Commun.*, 2024, **41**, 110245.
109 Y. Han, H. Zeng, H. Hao, H. Li, X. Niu, X. Liu, D. Zhang, L. Chen, W. Qi, H. Fan and K. Wang, *J. Colloid Interface Sci.*, 2025, **689**, 137207.
110 H. H. Jasim Al-Khafaji, A. Alsalamy, M. Abed Jawad, H. Ali Nasser, A. H. Dawood, S. Y. Hasan, I. Ahmad, M. A. Gatea and W. K. Younis Albahadly, *Front. Chem.*, 2023, **11**, 1236580.
111 M. Asiri, Y. Jawad BahrAluloom, M. Abdullateef Alzubaidi, I. Mourad Mohammed, M. Suliman, E. Ramzy Muhammad, A. S. Abed, F. Abodi Ali, S. K. Hadrawi, A. H. Alsalamy and M. Alwave, *Front. Mater.*, 2023, **10**, 1214426.
112 X.-P. Zhan, Y.-N. Zeng, B.-X. Li, H.-Q. Zheng, H.-X. Feng, Z. Xu, J. Liu and Z.-J. Lin, *Inorg. Chem.*, 2024, **63**, 677–688.
113 W. Zhang, B. Wang, G. Xiang, T. Jiang and X. Zhao, *ACS Appl. Mater. Interfaces*, 2023, **15**, 22830–22842.
114 A. R. Chowdhuri, B. Das, A. Kumar, S. Tripathy, S. Roy and S. K. Sahu, *Nanotechnology*, 2017, **28**, 095102.
115 X. Y. Song, Q. Jiang, J. Ma, Y. Liu, L. Zhang, T. Jiang, J. Zhang, Q. Li and J. Sun, *Ceram. Int.*, 2024, **50**, 7486–7496.
116 C. Y. Hsu, I. Kaur, E. Ali, Y. A. Naeem, F. Alajeeli, N. K. Younis, A. N. Faisal, I. H. Mohammed, N. Khalil, M. A. Jawad, M. A. M. Hussein, I. Ahmad, A. Elawady and A. Alsalamy, *J. Organomet. Chem.*, 2024, **1010**, 123111.
117 H. S. Rodríguez, J. P. Hinestroza, C. Ochoa-Puentes, C. A. Sierra and C. Y. Soto, *J. Appl. Polym. Sci.*, 2014, **131**, 40815.
118 C. Willyard, *Nature*, 2017, **543**, 15.
119 S. A. Polash, T. Khare, V. Kumar and R. Shukla, *ACS Appl. Bio Mater.*, 2021, **4**, 8060–8079.
120 S. Gui, X. Li, M. Feng, H. Liu, L. Huang and X. Niu, *Front. Bioeng. Biotechnol.*, 2023, **11**, 1166790.
121 P. Raju, T. Ramalingam, T. Nooruddin and S. Natarajan, *J. Drug Delivery Sci. Technol.*, 2020, **56**, 101560.
122 B. Mortada, T. Abou Matar, A. Sakaya, H. Atallah, Z. K. Ali, P. Karam and M. Hmadeh, *Inorg. Chem.*, 2017, **56**, 4739–4744.

123 S. Soltani and K. Akhbari, *JBIC, J. Biol. Inorg. Chem.*, 2022, **27**, 81–87.
124 H. Wei, Y. Luo, C. Wang, S. Wu, Y. Zheng, Y. Zhang, J. Shen and X. Liu, *Small Methods*, 2023, **7**, 2201618.
125 C. Liu, X. Zhao, Z. Wang, Y. Zhao, R. Li, X. Chen, H. Chen, M. Wan and X. Wang, *J. Nanobiotechnol.*, 2023, **21**, 427.
126 M. Wang, H. Huang, X. Ma, C. Huang and X. Peng, *Int. J. Biol. Macromol.*, 2021, **187**, 699–709.
127 R. F. Hamarawf, *RSC Adv.*, 2024, **14**, 9080–9098.
128 H. Zheng, B. Zhong, Q. Wang, X. Li, J. Chen, L. Liu and T. Liu, *Int. J. Mol. Sci.*, 2023, **24**, 12238.
129 R. Roudbari, N. Keramati and M. Ghorbani, *J. Mol. Liq.*, 2021, **322**, 114524.
130 X. Unamuno, E. Imbuluzqueta, F. Salles, P. Horcajada and M. J. Blanco-Prieto, *Eur. J. Pharm. Biopharm.*, 2018, **132**, 11–18.
131 M. Shen, X. Liao, Y. Xianyu, D. Liu and T. Ding, *ACS Appl. Mater. Interfaces*, 2022, **14**, 12662–12673.
132 Haseena, A. Khan, F. Aslam, T. Kanwal, M. R. Shah, A. A. K. Khalil, S. W. A. Shah, E. M. Alshammari, E. A. El-Masry, G. E.-S. Batiha and R. S. Baty, *Antibiotics*, 2021, **10**, 1071.
133 A. Arenas-Vivo, V. Celis Arias, G. Amariei, R. Rosal, I. Izquierdo-Barba, T. Hidalgo, M. Vallet-Regí, H. I. Beltrán, S. Loera-Serna and P. Horcajada, *Pharmaceutics*, 2023, **15**, 301.